

2

AD-A207 768

**RESPONSE FUNCTIONS OF A BC501  
SCINTILLATION DETECTOR FOR NEUTRONS  
UP TO 41 MeV**

R. R. Kiziah  
M. P. Snell



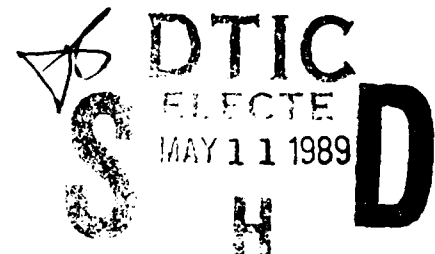
April 1989

Final Report

**A  
F  
W  
L**

Approved for public release; distribution unlimited.

**AIR FORCE WEAPONS LABORATORY**  
Air Force Systems Command  
Kirtland Air Force Base, NM 87117-6008

**DTIC**  
ELECTE  
MAY 11 1989

UNCLASSIFIED

SECURITY CLASSIFICATION OF THIS PAGE

REPORT DOCUMENTATION PAGE				Form Approved OMB No. 0704-0188	
1a. REPORT SECURITY CLASSIFICATION Unclassified			1b. RESTRICTIVE MARKINGS		
2a. SECURITY CLASSIFICATION AUTHORITY			3. DISTRIBUTION / AVAILABILITY OF REPORT Approved for public release; distribution unlimited.		
2b. DECLASSIFICATION / DOWNGRADING SCHEDULE					
4. PERFORMING ORGANIZATION REPORT NUMBER(S) AFWL-TR-88-83			5. MONITORING ORGANIZATION REPORT NUMBER(S)		
6a. NAME OF PERFORMING ORGANIZATION Air Force Weapons Laboratory		6b. OFFICE SYMBOL (if applicable) AWYW	7a. NAME OF MONITORING ORGANIZATION		
6c. ADDRESS (City, State, and ZIP Code) Kirtland Air Force Base, New Mexico 87117-6008			7b. ADDRESS (City, State, and ZIP Code)		
8a. NAME OF FUNDING / SPONSORING ORGANIZATION		8b. OFFICE SYMBOL (if applicable)	9. PROCUREMENT INSTRUMENT IDENTIFICATION NUMBER		
8c. ADDRESS (City, State, and ZIP Code)			10. SOURCE OF FUNDING NUMBERS		
			PROGRAM ELEMENT NO. 63224C	PROJECT NO. LTH4	TASK NO. 03
					WORK UNIT ACCESSION NO. 30
11. TITLE (Include Security Classification) RESPONSE FUNCTIONS OF A BC501 SCINTILLATION DETECTOR FOR NEUTRONS UP TO 41 MeV					
12. PERSONAL AUTHOR(S) Kiziah, Rex R.; Snell, Michael P.					
13a. TYPE OF REPORT Final		13b. TIME COVERED FROM 03/85 TO 12/87		14. DATE OF REPORT (Year, Month, Day) 1989, April	
				15. PAGE COUNT 70	
16. SUPPLEMENTARY NOTATION					
17. COSATI CODES			18. SUBJECT TERMS (Continue on reverse if necessary and identify by block number)		
FIELD	GROUP	SUB-GROUP	Response Function		
18	04		Scintillator		
20	06		Neutron Detector		
			Time-of-Flight		
19. ABSTRACT (Continue on reverse if necessary and identify by block number)					
<p>Using time-of-flight and pulse-shape discrimination techniques, the response functions of a 5-cm-long by 5-cm-diam BC501 liquid organic scintillation detector were measured for nearly monoenergetic neutrons at 43 energies between 2 and 41 MeV. Absolute normalization of the neutron pulse-height distributions for energies less than 31 MeV was performed by matching the largest pulse-height regions, the proton-recoil plateaus, of the distributions to Monte Carlo calculations of the detector response. The remaining distributions were normalized through comparison of experimental and calculated integral efficiencies. The 32 BC501 neutron response functions at energies between 2 and 22 MeV agree well with published response functions of a 4.60-cm-long by 4.65-cm-diam NE213 scintillation detector when simple corrections are applied for differences in density, composition, size, and normalizing cross-sectional area between the detectors. This set of BC501 response functions is to be used for construction of a detailed response matrix for unfolding neutron pulse-height distributions up to energies of 41 MeV. With (over)</p>					
20. DISTRIBUTION / AVAILABILITY OF ABSTRACT <input checked="" type="checkbox"/> UNCLASSIFIED/UNLIMITED <input type="checkbox"/> SAME AS RPT. <input type="checkbox"/> DTIC USERS			21. ABSTRACT SECURITY CLASSIFICATION Unclassified		
22a. NAME OF RESPONSIBLE INDIVIDUAL Captain Jeffrey B. Martin			22b. TELEPHONE (Include Area Code) (505) 844-1871		22c. OFFICE SYMBOL AWYW

DD Form 1473, JUN 86

Previous editions are obsolete.

SECURITY CLASSIFICATION OF THIS PAGE

UNCLASSIFIED

UNCLASSIFIED

SECURITY CLASSIFICATION OF THIS PAGE

19. ABSTRACT (Continued)

simple scale adjustments, the response functions can also be used for unfolding pulse-height distributions acquired with an equal-sized NE213 scintillation detector.

UNCLASSIFIED

SECURITY CLASSIFICATION OF THIS PAGE

## ACKNOWLEDGMENTS

We thank R. T. Santoro at Oak Ridge National Laboratory (ORNL), Oak Ridge, Tenn., for his efforts in arranging for these response function measurements to be made at the Oak Ridge Electron Linear Accelerator (ORELA) facility. Much thanks go to N. W. Hill, R. R. Spencer, and J. K. Dickens at ORNL for their help in conducting the experiment and performing the Monte Carlo calculations. We also express our appreciation for the support from the operational staff of the ORELA facility. Lastly, we are grateful to C. A. Goulding at Los Alamos National Laboratory, Los Alamos, N. Mex., for assistance during the experiment and for helpful discussions throughout processing of the data.



Accession For	
NTIS GRA&I	<input checked="checked" type="checkbox"/>
DTIC TAB	<input type="checkbox"/>
Unannounced	<input type="checkbox"/>
Justification	
By	
Distribution/	
Availability Codes	
Dist. Special	
A-1	

## CONTENTS

INTRODUCTION	1
DESCRIPTION OF THE BC501 SCINTILLATION DETECTOR	4
EXPERIMENTAL TECHNIQUE	6
DATA ANALYSIS	12
General	12
Method of pulse-height scale calibration	12
Method of normalization	21
Comparison of the BC501 neutron response functions to the Ref. 1 response functions	21
RESULTS AND DISCUSSION	24
REVIEW AND CONCLUSIONS	26
REFERENCES	27
APPENDIXES	
A. DETERMINING THE PROTON LIGHT-OUTPUT FUNCTION, $L(E_p)$ , FROM MEASURED MONOENERGETIC NEUTRON PULSE-HEIGHT DISTRIBUTIONS	29
B. METHOD OF CONVERTING RESPONSE FUNCTIONS OF A 4.60-CM-LONG BY 4.65-CM-DIAM NE213 SCINTILLATION DETECTOR TO RESPONSE FUNCTIONS OF A 5-CM-LONG BY 5-CM-DIAM BC501 SCINTILLATION DETECTOR	32
C. ABSOLUTE DIFFERENTIAL EFFICIENCY CURVES FOR THE 5-CM-LONG BY 5-CM-DIAM BC501 SCINTILLATION DETECTOR FOR NEUTRON ENERGIES BETWEEN 2 AND 41 MeV	37
D. TABULATION OF ABSOLUTE DIFFERENTIAL EFFICIENCY VERSUS PULSE HEIGHT OF A 5-CM-LONG BY 5-CM-DIAM CYLINRICAL BC501 SCINTIL- LATION DETECTOR FOR MONOENERGETIC NEUTRONS INCIDENT ON THE TOP, FLAT FACE OF THE SCINTILLATOR	45

## LIST OF FIGURES

<u>Figure</u>		<u>Page</u>
1	Schematic of the BC501 scintillation detector.	5
2	Block diagram of the data acquisition electronics.	7
3	An example of the pulse-shape discrimination obtained using an $^{241}\text{Am}$ - $^9\text{Be}$ source with a discrimination level of 330 keV equivalent electron energy applied. (Neutron events are on the right; gamma-ray events are on the left. The zero of the x-axis is arbitrary.)	8
4	Pulse-shape spectra acquired during the neutron response function measurements for four different pulse-height regions. (P refers to pulse height and $E_p$ refers to the proton energy corresponding to P. Events to the left of the vertical line are gamma rays; events to the right are neutrons.)	10
5	A measured pulse-height spectrum for the 5-cm-long by 5-cm-diam BC501 scintillation detector for the 0.511- and 1.275-MeV gamma rays from a $^{22}\text{Na}$ source. ( $L_{\text{max}}$ , $L_{1/2}$ , and $L$ are the positions of the maximums, half heights, and Compton edges, respectively, of the Compton electron spectra.)	13
6	Maximum Compton electron energy versus channel number for the 5-cm-long by 5-cm-diam BC501 scintillation detector. (The solid line is a least-squares fit to the data yielding $E_e = 9.98 \times 10^{-3} \times \text{channel no.} + 4.67 \times 10^{-2}$ , in MeV.)	14
7	Unnormalized neutron pulse-height distributions for the 5-cm-long by 5-cm-diam BC501 scintillation detector. (The solid curves are fits to the edges of the distributions which define the pulse heights corresponding to the maximum proton energies $E_p = E_n$ .)	16
8	Pulse height versus proton energy for the 5-cm-long by 5-cm-diam BC501 scintillation detector (filled circles) and the 4.60-cm-long by 4.65-cm-diam NE213 scintillation detector of Ref. 1 (solid curve). (Error bars are shown only for every other data point.)	17
9	Saturated (solid curve) and saturation-corrected (chain-dashed curve) neutron pulse-height distributions for $E_n = 30.2$ MeV for the 5-cm-long by 5-cm-diam BC501 scintillation detector.	18

## LIST OF FIGURES (Continued)

<u>Figure</u>		<u>Page</u>
10	Pulse-height resolution as a function of pulse height for the 5-cm-long by 5-cm-diam BC501 scintillation detector determined from monoenergetic neutron distributions (filled circles) and monoenergetic gamma-ray distributions (filled squares). (Error bars are shown only for every other data point.)	19
11	Energy resolution as a function of neutron energy for the 5-cm-long by 5-cm-diam BC501 scintillation detector determined from monoenergetic neutron distributions. (Error bars are shown only for every other data point.)	20
12	Absolute differential efficiency curves for the 5-cm-long by 5-cm-diam BC501 scintillation detector (solid curves) and the 4.60-cm-long by 4.65-cm-diam NE213 scintillation detector (dashed curves) of Ref. 1 corrected for the differences in density, composition, size, and normalizing cross-sectional area.	23

## INTRODUCTION

Since the early 1960s, liquid organic scintillators have been used extensively for fast neutron ( $> 100$  keV) spectroscopy because of their desirable characteristics: high neutron detection efficiency, no dependence of the light output on the incident neutron direction, fast time response, discrimination against gamma-ray backgrounds, and good pulse-height resolution. Of the liquid organic scintillators, NE213 is the most widely used and is the standard scintillator for fast neutron spectroscopy, especially for those measurements in which the neutron energy spectra cannot be determined by time-of-flight (TOF) techniques. NE213 possesses excellent pulse-shape discrimination (PSD) properties (different scintillation light pulse shapes for different charged particles) which make it suitable for neutron measurements accompanied by gamma-ray backgrounds. Also, the papers by Verbinski, et al (Ref. 1) and Burrus and Verbinski (Ref. 2) provided the detailed neutron response functions and methodology needed for determining incident neutron energy spectra from pulse height distributions measured with a nominal 5-cm-long by 5-cm-diam cylindrical NE213 scintillator. Neutron spectra were derived with an energy resolution of  $\approx 10$  percent. As a result, the standard 5-cm-long by 5-cm-diam NE213 scintillator has been used as a neutron spectrometer for a wide variety of measurements in which TOF techniques could not be employed. A few examples are the measurement of time-dependent fast neutron spectra of pulsed small assemblies (Ref. 3), secondary neutron production cross sections for testing the accuracy of evaluated neutron data files (Ref. 4), neutron fluxes from tokamak plasma devices (Refs. 5 and 6), neutron energy spectra from photo-nuclear reactions (Ref. 7), neutron elastic and inelastic differential cross sections (Ref. 8) and neutron energy spectra from particle bombardment of thick elemental targets (Ref. 9).

In recent years, the BC501 scintillator manufactured by Bicron Corporation, in Newbury, Ohio has been sold as a replacement for the NE213 scintillator. The primary difference between the two scintillators is the scintillation solvent. BC501 contains pseudocumene and has a flash point of  $47^{\circ}\text{C}$ ; NE213 is based on xylene, resulting in a flash point of  $26^{\circ}\text{C}$ . Thus, BC501 is safer when used in large volumes and is safer to ship. Concerning fast neutron detection and neutron/gamma-ray discrimination, the BC501 and NE213 scintillators are similar. The density of BC501 is  $0.901\text{ g/cm}^3$  with a chemical composition of  $\text{CH}_{1.287}$  (Ref. 10). The density and composition of NE213 are  $0.874\text{ g/cm}^3$  and



CH<sub>1.212</sub>, respectively (Ref. 11). Therefore, for the same size scintillator cells, BC501 has a slightly higher neutron detection efficiency than NE213. Also, the light output, or scintillation efficiency, of BC501 is slightly higher than that of NE213, 80 percent of the light output of the crystalline organic scintillator anthracene as compared to 78 percent, possibly resulting in a slight improvement in energy resolution.

As part of an extensive study to investigate neutron production by charged particle bombardment of elemental and multimaterial targets, a 5-cm-long by 5-cm-diam cylindrical BC501 scintillation detector was acquired for the measurement of neutron energy spectra in the range of  $\approx 0.5$  to 40 MeV. Some of the measurements were made at accelerator facilities which did not allow TOF detection of the neutron spectra; therefore, the neutron energy spectra were determined by applying unfolding methods to measured pulse-height distributions. Because BC501 was a new replacement for NE213, there was no literature describing BC501's response to fast neutrons or its PSD properties. Although one could assume that the neutron response characteristics of BC501 are almost identical to those of NE213 since their physical properties are so similar, a measurement of the response functions of our BC501 scintillation detector for nearly monoenergetic neutrons at energies between  $\approx 2$  and 41 MeV was determined as necessary. One reason for the set of measurements was that there were no published experimental response functions to neutrons  $> 22$  MeV for the standard 5-cm-long by 5-cm-diam NE213 scintillator. In addition, after examination of the literature concerning Monte Carlo calculations of neutron response functions, it was clear that such calculations were inaccurate representations of the responses at the low pulse-height regions for neutron energies  $> 20$  MeV. Lastly, as noted by Pieroni, et al (Ref. 3) and Perkins (Ref. 12), standard published results, e.g., (Ref. 1), may not be directly applicable to every 5-cm-long by 5-cm-diam NE213 scintillation detector as many authors have assumed. Both authors observed deviations from the Ref. 1 responses for their detector systems at the higher neutron energies, which they attributed to nonlinearities or saturation in the photomultiplier tubes.

In this report, results are presented for the TOF measurement of 43 neutron response functions for energies between 2 and 41 MeV. Since the number of neutrons in each energy group incident on the BC501 scintillator were not determined experimentally, the technique of Ref. 1 was used to normalize each

pulse-height distribution for the neutron energies  $< 31$  MeV. Experimental pulse-height spectra were normalized to the proton-recoil plateaus of calculated curves. The proton-recoil plateaus are the large pulse-height regions, resulting from neutron-hydrogen collisions, which the Monte Carlo calculations most accurately describe. The remaining pulse-height distributions were normalized to calculated integral efficiencies. The BC501 response functions are compared to the NE213 response functions reported in Ref. 1, and the NE213 response functions are used to extend the BC501 responses to lower pulse heights.

## DESCRIPTION OF THE BC501 SCINTILLATION DETECTOR

The BC501 liquid organic scintillation detector was obtained from Bicorn Corporation as an integral assembly. A schematic of the detector is shown in Fig. 1. The BC501 liquid was deoxygenated in a nitrogen atmosphere and placed in a hermetically sealed Bicrocell. The Bicrocell consists of an aluminum and glass cylinder with an inside diameter of 5.08 cm and length of 5.08 cm. The top, flat face of the aluminum cell is 1.6 mm thick, and the curved surface is 5.46 mm thick. The inside aluminum surfaces are coated with BC624, a white reflective paint. The bottom, flat face of the Bicrocell consists of a ground and polished 6.35-mm-thick Pyrex viewing port. An extrinsic reservoir containing oxygen-free nitrogen is provided to allow for volume changes of the liquid within the sealed Bicrocell. The extrinsic reservoir eliminates any contained bubbles of nitrogen gas within the volume of the liquid scintillator which could introduce a slight neutron response anisotropy. The viewing port of the Bicrocell is directly coupled to a Hamamatsu R329-02 photomultiplier tube (equivalent to RCA 8575 photomultiplier tube) with a light shield and a  $\mu$ -metal magnetic shield.

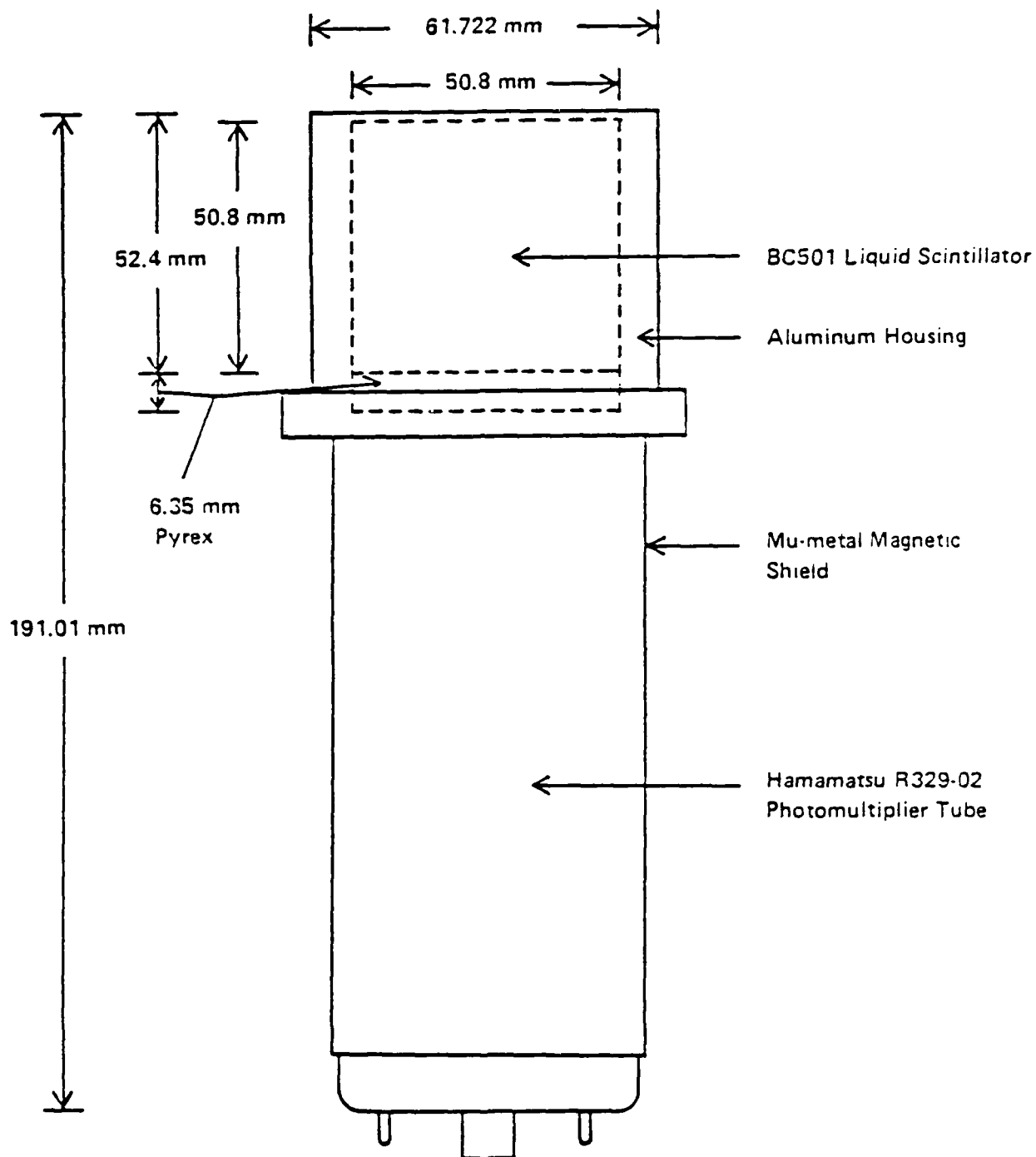


Figure 1. Schematic of the BC501 scintillation detector.  
(Schematic shown with permission of Bicron Corporation.)

## EXPERIMENTAL TECHNIQUE

The measurement of relative pulse-height distributions for neutrons as a function of incident energy for the BC501 scintillation detector was conducted at the 85-m flight station of the Oak Ridge Electron Linear Accelerator (ORELA) facility. High-energy electrons (100 to 180 MeV) incident on a tantalum converter produce a narrow beam of gamma rays which then generate neutrons by a  $(\gamma, n)$  reaction in a beryllium block. For this experiment, the electron beam pulse width was  $\approx 17$  ns full width at half maximum (FWHM) with a peak current of  $\approx 10$  A. The repetition rate was 800 Hz. With these electron-beam parameters, the detector counting rate was approximately one event (neutron or gamma ray) every eight pulses. The distance between the center of the beryllium block and the center of the BC501 scintillator was 86.9 m. Collimators in the 85-m flight path defined a parallel flux of neutrons with an  $\approx 5$ -cm-diam spot size at the detector. The detector was positioned so that the axes of the detector and neutron beam were collinear. A depleted uranium filter located after the beryllium block was used to reduce the intensity of the gamma flash. Also, a  $^{10}\text{B}$  filter followed the depleted uranium filter in order to remove low-energy neutrons which would overlap from one linac burst to the next.

Figure 2 is a block diagram of the data acquisition electronics used for the measurement of the neutron response functions. Three parameters were acquired and stored by a PDP-9 computer and the ORELA SEL810B computer for each detector event: pulse shape, pulse height, and TOF. The pulse-shape or rise-time parameter was derived from the PSD circuitry and was used to classify an event as a neutron or a gamma ray. An ORTEC 113 preamplifier, ORTEC 460 delay-line amplifier (DLA), ORTEC 552 pulse-shape analyzer (PSA), and ORTEC 467 time-to-amplitude converter (TAC) comprised the PSD circuitry. This combination of electronic modules was used because it formed the PSD electronics for previous neutron spectroscopy measurements. The PSD circuitry works in the following manner. The rise times of the signals from the preamplifier are different for gamma-ray and neutron events due to the different scintillation responses of BC501 to recoiling electron and proton or heavier particle (alphas, deuterons, etc.) ionizations. Processing a preamplifier signal with the DLA (single delay-line mode, 1- $\mu\text{s}$  delay line) results in a unipolar output pulse whose fall time corresponds to the rise time of the input pulse. The PSA generates two timing pulses, which are determined by the constant-fraction method, on the trailing edge of the input signal. The two reference fractions were taken at the 10-percent and 90-percent decay points of the peak pulse height.

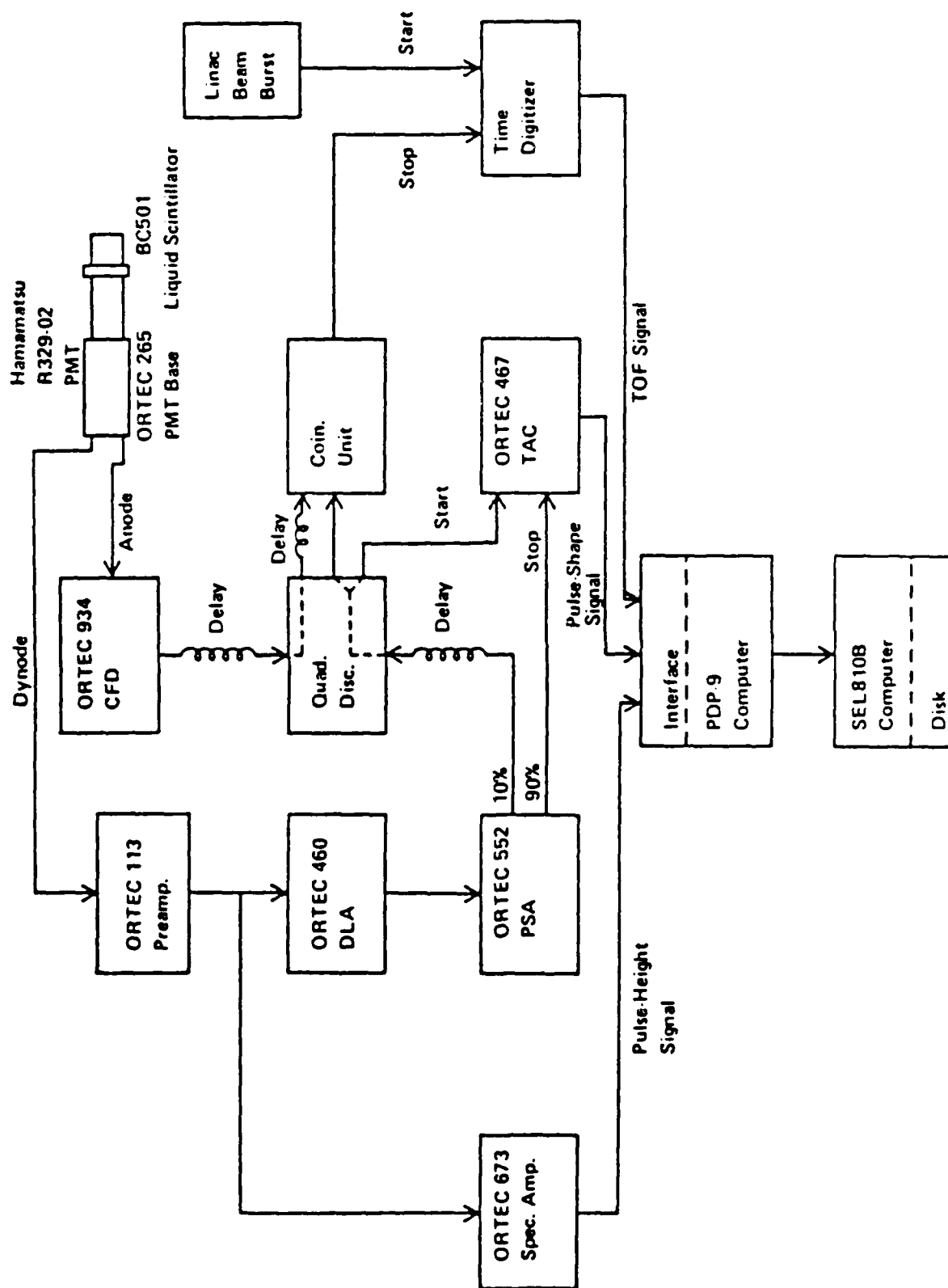


Figure 2. Block diagram of the data acquisition electronics.

During tests of the PSD electronics with an  $^{241}\text{Am}-^9\text{Be}$  mixed neutron/gamma-ray source, these fractions gave the best identification of neutron and gamma-ray events with minimal misclassification of events. The two timing signals drive the TAC, which produces an output signal whose amplitude is proportional to the rise time of the preamplifier signal. Digitizing the TAC signals results in a pulse-shape spectrum such as that shown in Fig. 3. Figure 3 shows the distribution of rise times for neutron and gamma-ray events from an  $^{241}\text{Am}-^9\text{Be}$  source, with the PSA discriminator level set to accept only neutron- and gamma-ray-event signals with pulse heights greater than or equal to the pulse height which would be produced by 330-keV electrons. The gamma-ray-event distribution (left peak) has a FWHM of 4.6 ns. The FWHM of the neutron-event-distribution (right peak) is 38 ns and the maximums of the two distributions are separated by 60 ns. The neutron peak-to-valley ratio is 50. Thus, the quality of neutron/gamma-ray discrimination is good.

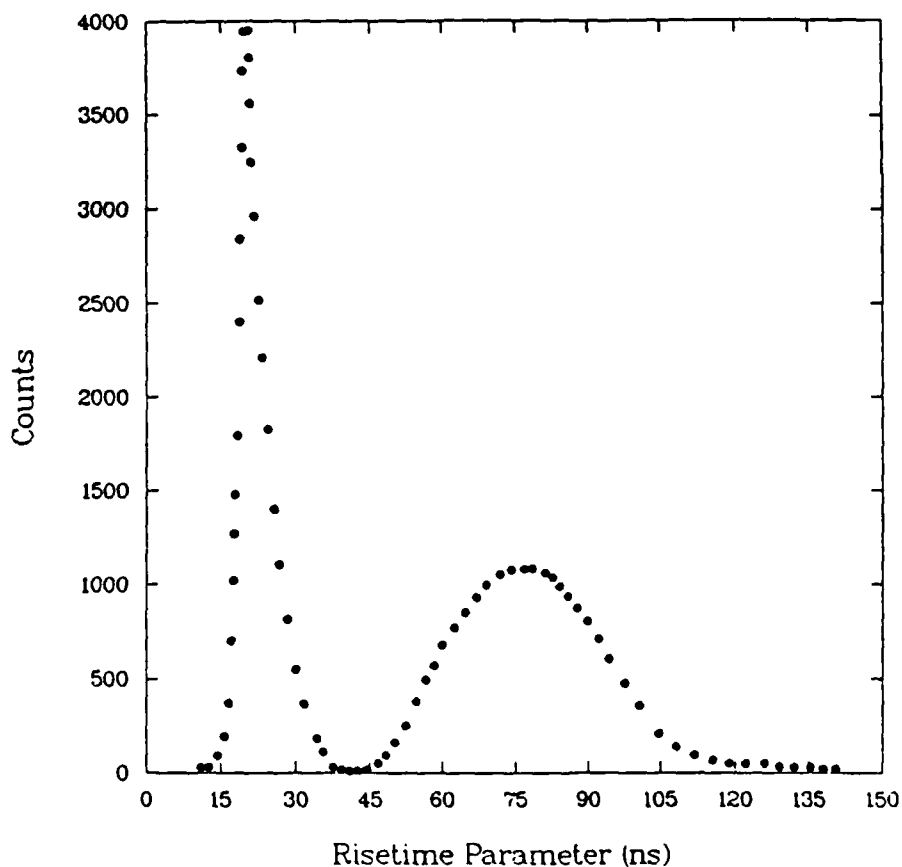


Figure 3. An example of the pulse-shape discrimination obtained using an  $^{241}\text{Am}-^9\text{Be}$  source with a discrimination level of 330 keV equivalent electron energy applied. (Neutron events are on the right; gamma-ray events are on the left. The zero of the x-axis is arbitrary.)

During the neutron response function measurements, pulse-shape spectra were acquired for a series of eight pulse-height regions. The PSA discriminator level was set to a pulse height which would be produced by 200-keV electrons; thus, neutrons below 1 MeV were not processed by the electronics. Multiple pulse-height regions enabled the pulse-shape parameter to be determined as a function of pulse height, which is necessary since the rise time of an event, especially for a neutron, varies as a function of the pulse height. In addition, in certain pulse-height ranges, neutron- and gamma-ray event signals can have the same rise times. These effects, combined with timing resolution and pulse-height resolution effects, makes neutron and gamma-ray separation based only on rise times difficult over the very large range of pulse heights associated with 1- to 41-MeV neutrons. Pulse-shape spectra for four pulse-height regions are shown in Fig. 4. Both the neutron and gamma-ray rise time distribution change with pulse height. The vertical line in each spectrum defines the division of neutron and gamma-ray events. This division was chosen separately for each pulse-height region. An event with a pulse-shape parameter to the right of the vertical line was classified as a neutron. Evident in the highest pulse-height pulse-shape spectra are two distributions right of the vertical line. The distribution farthest to the right is due to alphas produced from  $^{12}\text{C}(\text{n},\alpha)^9\text{Be}$  and  $^{12}\text{C}(\text{n},\text{n}')3\alpha$  reactions. An event with a pulse-shape parameter left of the vertical line was classified as a gamma ray. The small number of gamma-ray events are due to both gamma-ray contamination in the neutron flux (gamma rays produced in the tantalum converter and beryllium block combination) and gammas induced in the detector by neutrons, primarily 4.4-MeV gammas from  $^{12}\text{C}(\text{n},\text{n}')^{12}\text{C}^*$  reactions in the scintillator. The gamma rays in the neutron flux could have been identified as gamma rays through TOF. The induced gamma rays are actually part of the neutron response of the scintillator and are eliminated from our measured responses by the PSD electronics. Thus, the PSD electronics were not needed for the response function measurements but were used because they had been employed during prior neutron spectroscopy experiments. The data from these experiments would be analyzed with these response functions. However, it is important to note that the response functions can be used to unfold pulse-height distributions acquired without PSD, because the maximum correction to apply to the response functions for the elimination of the 4.4-MeV gammas is  $\approx 3$  percent.

The pulse-height parameter was a digitized signal also derived from the pre-amplifier signal, as shown in Fig. 2. After being shaped and amplified with a DLA, the preamplifier signal was processed with an ORTEC 673 spectroscopy



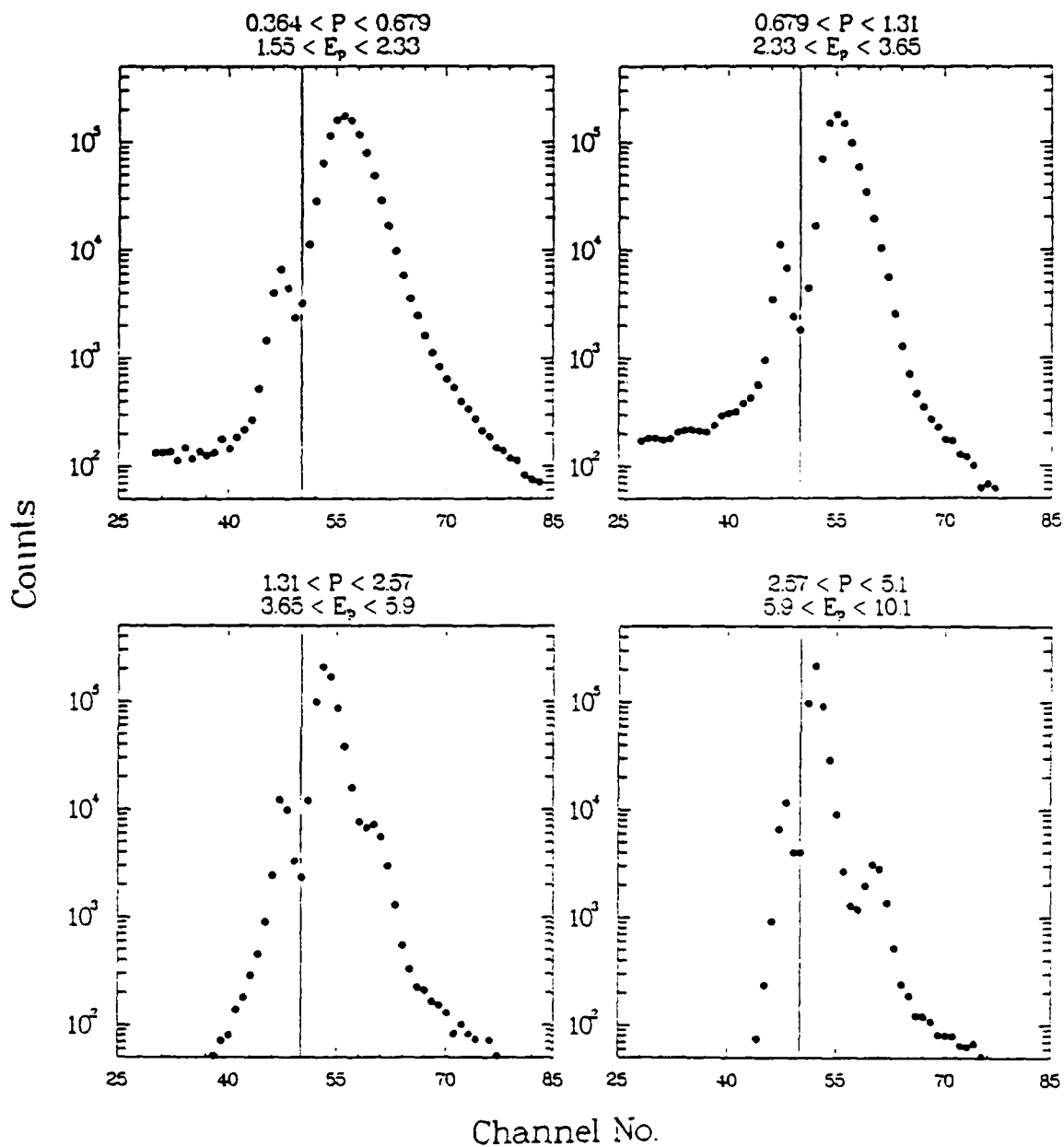


Figure 4. Pulse-shape spectra acquired during the neutron response function measurements for four different pulse-height regions. ( $P$  refers to pulse height and  $E_p$  refers to the proton energy corresponding to  $P$ . Events to the left of the vertical line are gamma rays; events to the right are neutrons.)

amplifier. The amplitude of the unipolar output pulse from the spectroscopy amplifier defined the pulse-height parameter.

As illustrated in Fig. 2, the TOF parameter was derived from the time difference between a linac beam burst and the detection of an event in the detector. The fast anode signal from the detector was input to an ORTEC 934 constant-fraction discriminator (CFD). The CFD discriminator level was set to a lower value than the PSA discriminator level. The timing signal from the CFD was coincided with a timing signal from the PSA so that TOF spectra were generated only for events which had been pulse-shape analyzed. The output signal from the coincidence unit served as the stop signal to a time digitizer (clock) while the start signal came from the linac beam pulse.

The pulse-shape, pulse-height, and TOF signals were processed by the PDP-9 computer and transferred with appropriate tags to the ORELA SEL810B computer for storage in two-parameter arrays of pulse height versus TOF and in one-parameter high-resolution TOF arrays. For example, the pulse-height and pulse-shape parameters were examined by the PDP-9 to determine whether an event was due to a neutron or gamma ray. If the event was a neutron, it was stored in the neutron two-parameter pulse height versus TOF array and neutron high-resolution TOF array. The same procedure was followed for a gamma-ray event.

## DATA ANALYSIS

GENERAL

The two-parameter array of pulse height versus TOF for events classified as neutrons was separated into 43 unnormalized pulse-height distributions. Each pulse-height distribution corresponded to a bin of neutron energies, determined from TOF, in which the bin width was  $\approx 7$  percent of the center neutron energy. The procedure for conversion of the unnormalized pulse-height distributions to neutron response functions or absolute differential efficiencies was to place each pulse-height distribution on a calibrated pulse-height scale and then normalize the distributions to one neutron incident on the cross-sectional area of the BC501 scintillation detector.

METHOD OF PULSE-HEIGHT SCALE CALIBRATION

Calibration of the pulse-height axis of each distribution was performed as follows. For organic scintillators, the light output or pulse height for a heavily ionizing particle such as a proton is a nonlinear function of the proton energy. However, the light output function for electrons is linear for electron energies  $> 100$  keV and may be expressed as  $L = c(E_e - E_0)$ , where  $L$  is the relative light output,  $E_e$  the electron energy,  $E_0$  the energy intercept, and  $c$  is a scaling parameter (Ref. 13). Thus, the first step towards energy calibration is to establish a reliable light-output function  $L(E_e)$  for electrons. Then the light output for protons  $L(E_p)$  is measured relative to the light output for electrons.

A convenient means of establishing  $L(E_e)$  is to use as calibration points the Compton edges of electron spectra resulting from gamma-ray interactions in the scintillator. The maximum Compton electron energy given by  $E_e = 2E_\gamma^2 / (2E_\gamma + 0.511 \text{ MeV})$ , where  $E_\gamma$  is the gamma-ray energy in MeV, is directly related to the Compton edge of the measured gamma-ray pulse-height distribution. However, multiple scattering and statistical fluctuations smear the theoretically sharp Klein-Nishina distribution; as a result, defining the Compton edge position from a measured spectrum varies among authors. The most accurate method of defining the Compton edge position is to compare a measured spectrum with a Monte Carlo calculation of the spectrum. Monte Carlo calculations were not performed for this work; the results of Dietz and Klein (Ref. 14) were used instead. In their paper they tabulated values of  $L_{\max}/L_c$  and  $L_{1/2}/L_c$  versus

detector resolution  $\Delta L/L$  for four sizes of NE213 scintillators, with one of the sizes examined corresponding to a 5-cm-long by 5-cm-diam detector. Their table was constructed from detailed Monte Carlo calculations. Referring to Fig. 5, which is a pulse-height distribution from the BC501 scintillation detector for gamma rays from a  $^{22}\text{Na}$  source,  $L_{\text{max}}$  is the position of the maximum of the distribution for a particular gamma ray,  $L_{1/2}$  is the half-height position, and  $L_c$  is the position of the Compton edge.  $L_{\text{max}}$  and  $L_{1/2}$  were determined for each of three gamma-ray pulse-height distributions, 0.511- and 1.275-MeV gamma rays from a  $^{22}\text{Na}$  source and 2.614-MeV gamma rays from a  $\text{ThC}''$  source, measured periodically during the neutron response function measurements. The resolution was determined from the estimate (Ref. 14)  $\Delta L/L = 1.5(L_{1/2} - L_{\text{max}})/L_{1/2}$ . Dietz and Klein found that this formula adequately described the resolution of their detectors, roughly independent of both gamma-ray energy and detector size. From the table and the measured resolutions, interpolation between tabulated resolutions determined  $L_{1/2}/L_c$  and thus

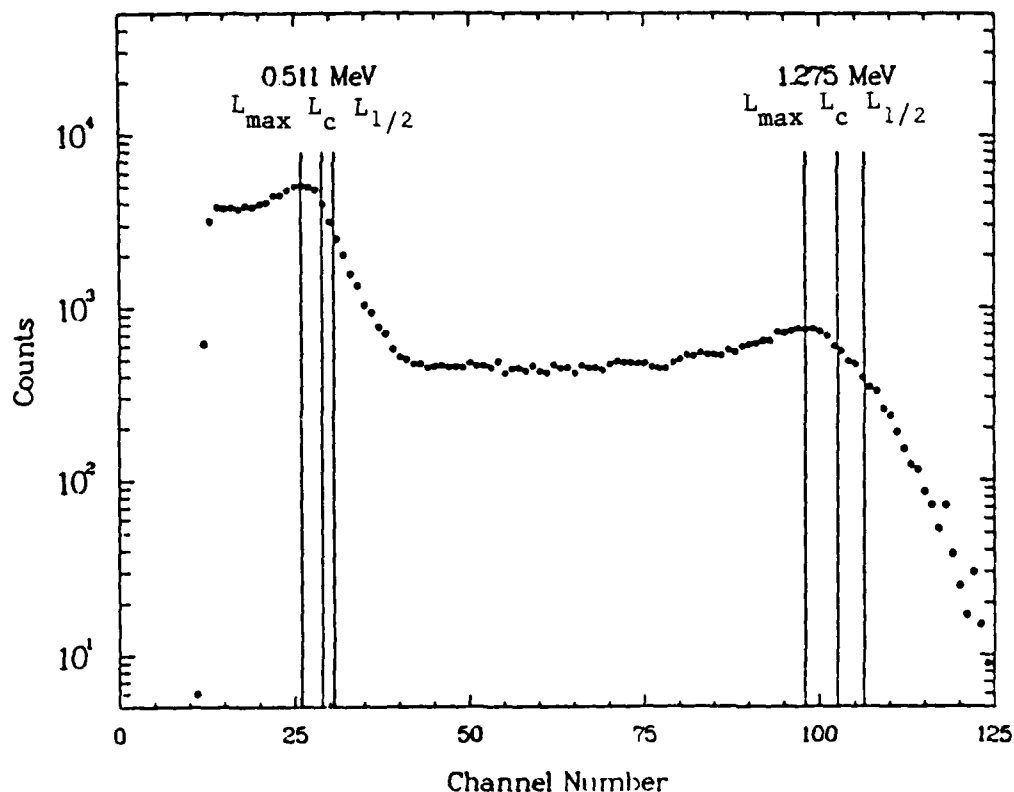


Figure 5. A measured pulse-height spectrum for the 5-cm-long by 5-cm-diam BC501 scintillation detector for the 0.511- and 1.275-MeV gamma rays from a  $^{22}\text{Na}$  source. ( $L_{\text{max}}$ ,  $L_{1/2}$ , and  $L_c$  are the positions of the maximums, half heights, and Compton edges, respectively, of the Compton electron spectra.)

$L_c$  for each Compton electron spectrum. A plot of channel numbers associated with the  $L_c$ 's versus the maximum Compton electron energies of 0.341, 1.062, and 2.381 MeV is shown in Fig. 6. Performing a least-squares fit to the data to determine the linear relationship between  $E_e$  and channel number and choosing the scaling parameter  $c$  as 1, resulted in a calibration of the pulse-height axis in terms of equivalent electron energy in MeV, commonly referred to as "MeVee."

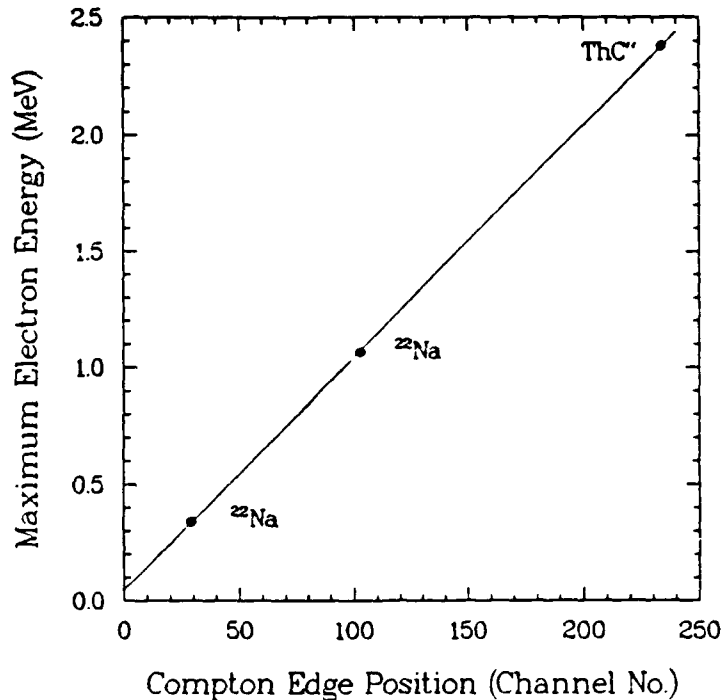


Figure 6. Maximum Compton electron energy versus channel number for the 5-cm-long by 5-cm-diam BC501 scintillation detector. (The solid line is a least-squares fit to the data yielding  $E_e = 9.98 \times 10^{-3} \times \text{channel no.} + 4.67 \times 10^{-2}$ , in MeV.)

With the pulse-height channel numbers placed on a calibrated light-output scale, the proton light-output function could be determined from the measured, nearly monoenergetic, neutron response functions. The procedure for establishing  $L(E_p)$  was similar to that of determining  $L(E_e)$ . The maximum proton energy  $E_p = E_n$ , where  $E_n$  is the midpoint energy of the TOF bin defining a given neutron response function, is directly related to the edge of the proton-recoil plateau region of the neutron pulse-height distribution (see Appendix A). However, due to multiple scattering, statistical fluctuations,

and nonisotropies in the n-p scattering process, care must be taken in defining the edge of the neutron pulse-height distribution. Figure 7 shows unnormalized pulse-height distributions for four neutron energies for the BC501 detector. The solid curve in each plot is a convolution (numerical integration) of a step function with a Gaussian function fitted to the edge of the distribution using the generalized minimization program MINUIT (Ref. 15) to determine the step value [which is  $L(E_p)$ ] and the FWHM of the Gaussian function. Only that region of data through which the curve passes was used in the fitting process so that the Gaussian-smoothed step function was a good approximation to the edge of the pulse-height distribution.

A plot of  $L(E_p)$  versus maximum proton energy determined from the edges of the neutron pulse-height distributions as described above is shown in Fig. 8. Also shown is the proton light-output function determined by Verbinski, et al, Ref. 1 for an NE213 scintillation detector. The light-output function of Ref. 1 was converted into units of MeVee using the equivalency 1 light unit = 1.22 MeVee, as determined in Ref. 14. This transformation corrected for the differences between Ref. 1 and this work in the location of the Compton edges of the electron spectra from gamma-ray sources used for calibration. There is very good agreement between the two light-output functions for proton energies < 10 MeV. Above 10 MeV, the proton light-output function for the BC501 scintillation detector deviates from the Ref. 1 curve, showing an increasingly smaller change in light output for increasing proton energy. This feature of the light-output function is characteristic of saturation of the pulse-height output signal of the detector. The cause of the saturation was most probably operation of the photomultiplier tube at too high an applied voltage. The saturation of the pulse-height signal has no effect on the measured neutron response functions except to fold a different nonlinearity into the proton light curve. Thus, each neutron pulse-height distribution was corrected for saturation by transforming on a channel-by-channel basis from the BC501 proton light curve to the Ref. 1 proton light curve. Figure 9 shows the result of this correction process for the 30.2-MeV neutron pulse-height distribution.

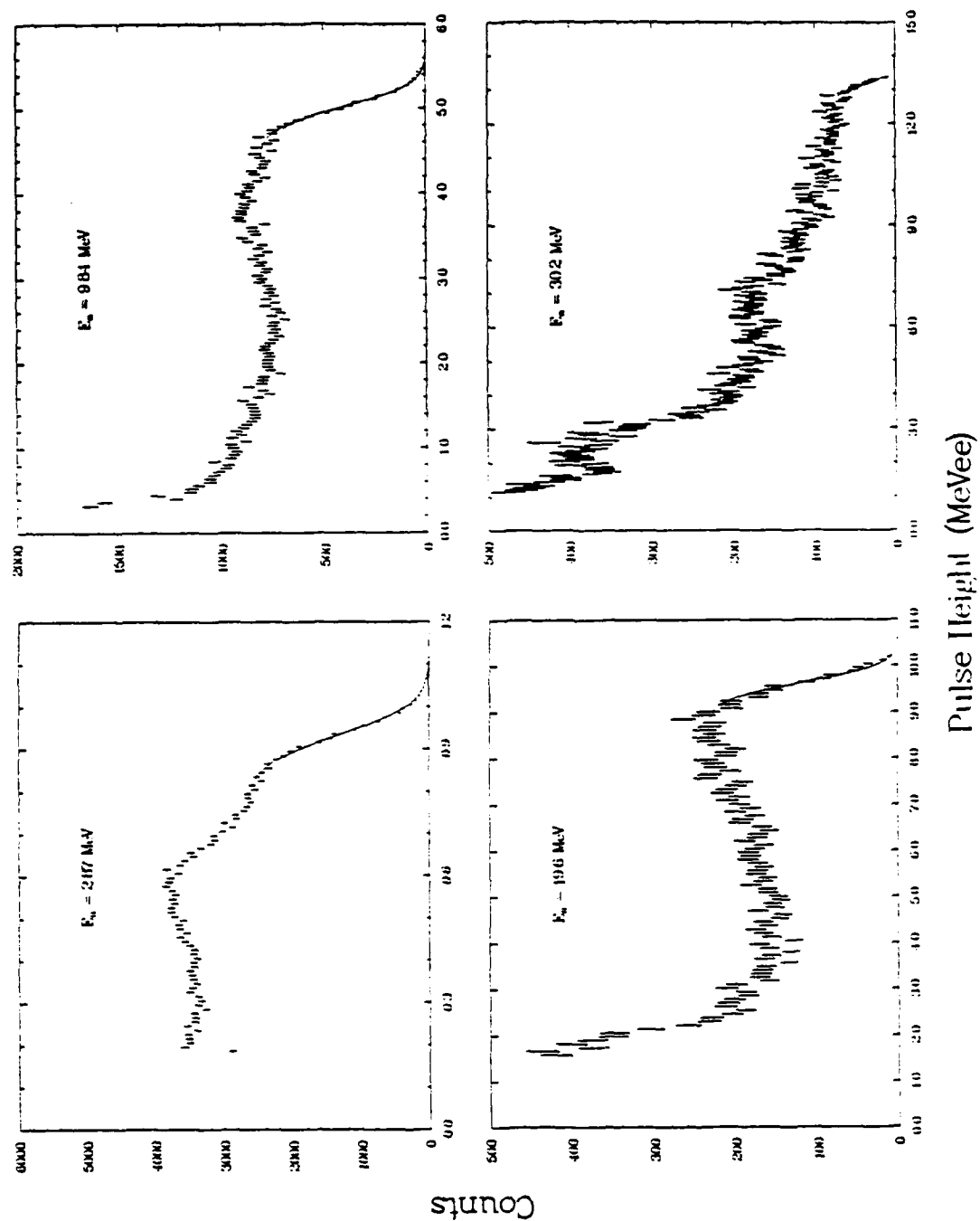


Figure 7. Unnormalized neutron pulse-height distributions for the 5-cm-long by 5-cm-diam BC501 scintillation detector. (The solid curves are fits to the edges of the distributions which define the pulse heights corresponding to the maximum proton energies  $E_p = E_n$ .)

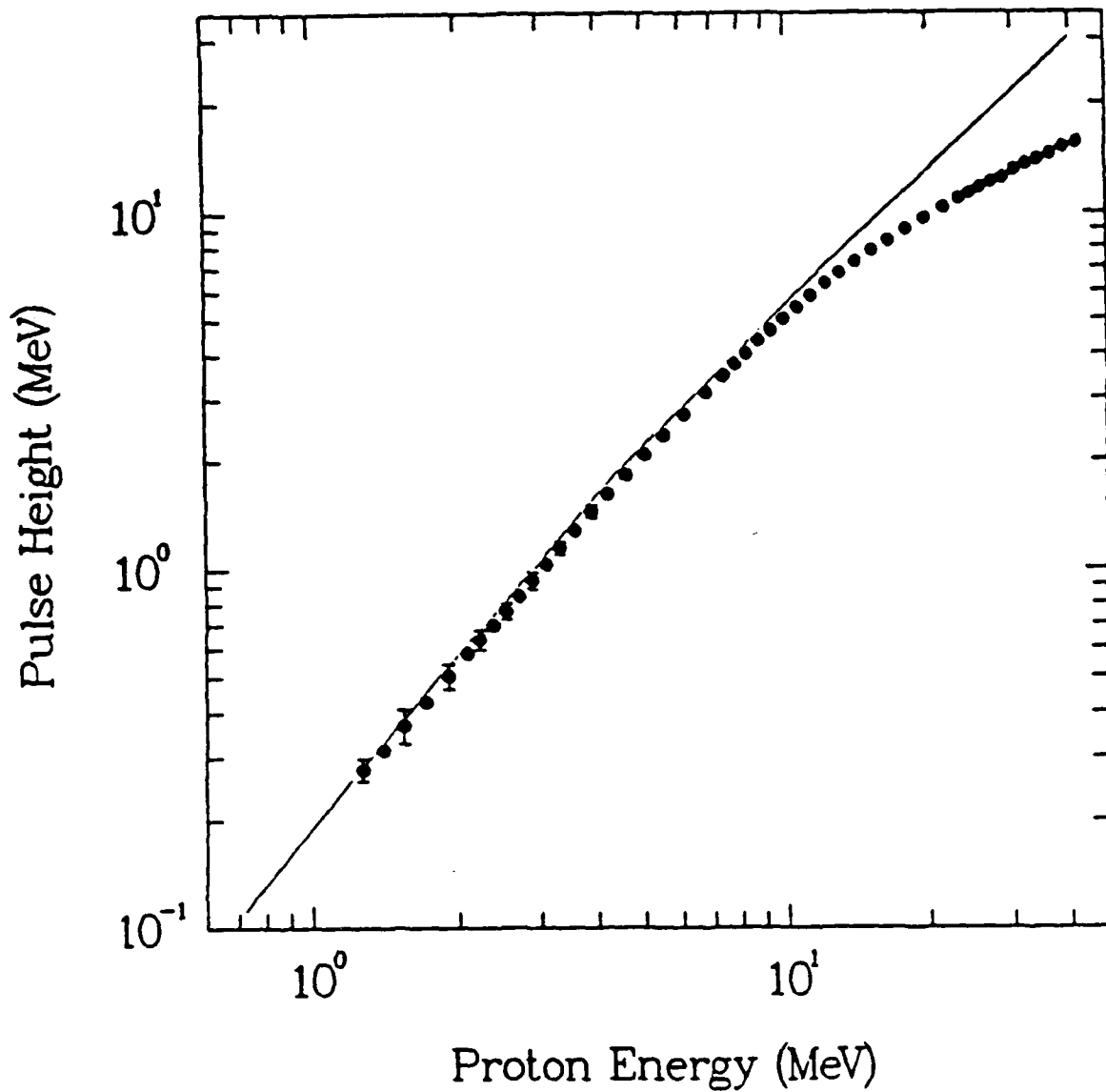


Figure 8. Pulse height versus proton energy for the 5-cm-long by 5-cm-diam BC501 scintillation detector (filled circles) and the 4.60-cm-long by 4.65-cm-diam NE213 scintillation detector of Ref. 1 (solid curve). (Error bars are shown only for every other data point.)



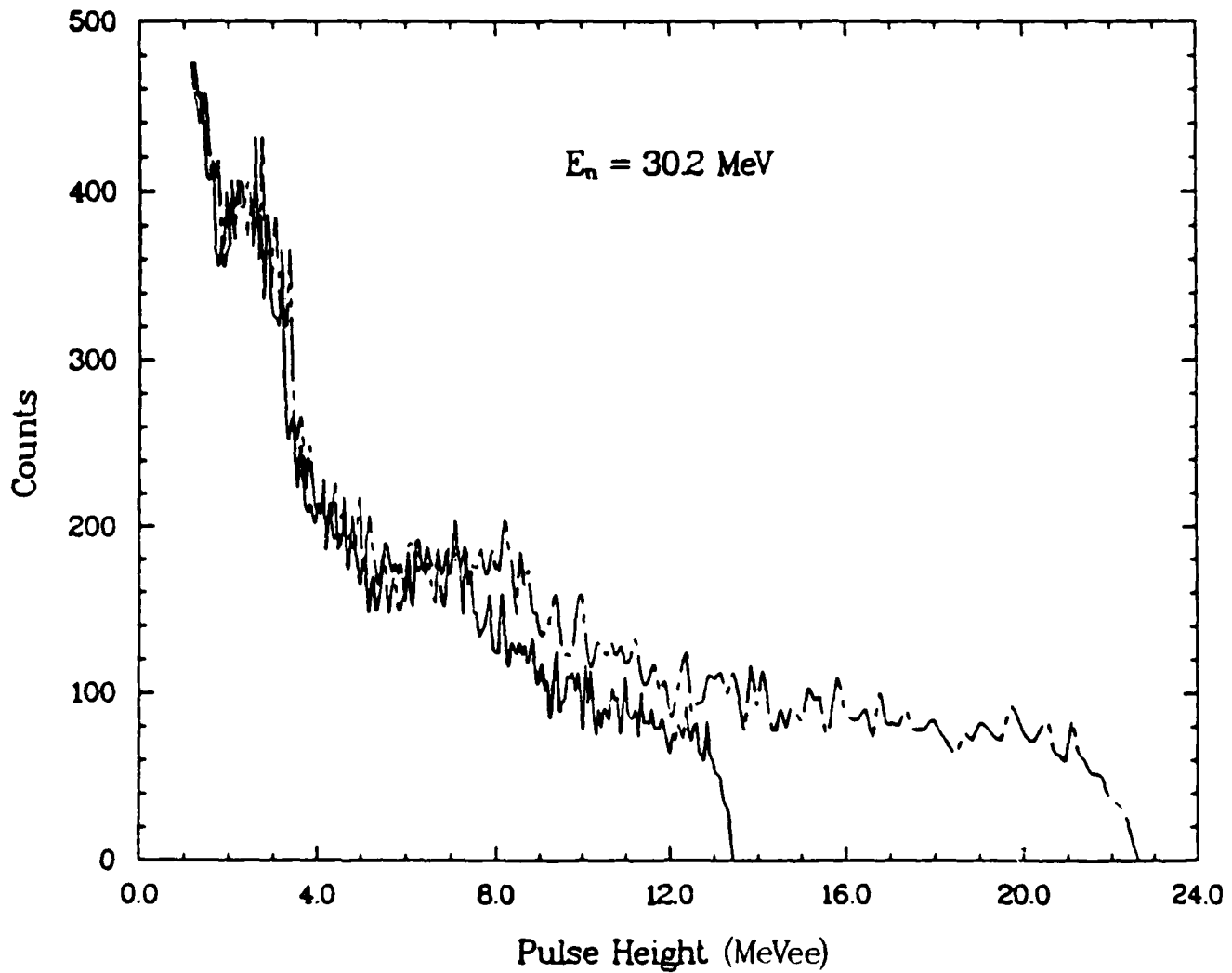


Figure 9. Saturated (solid curve) and saturation-corrected (chain-dashed curve) neutron pulse-height distributions for  $E_n = 30.2 \text{ MeV}$  for the 5-cm-long by 5-cm-diam BC501 scintillation detector.

Figure 10 is a plot of the pulse-height resolution  $\Delta L/L$  for the BC501 scintillation detector extracted from the edges of the neutron pulse-height distributions. The resolution values were determined from the fits to the saturated data and not from fits to the saturation-corrected pulse-height distributions. However, one should obtain nearly the same pulse-height resolution curve from the saturation-corrected distributions since  $\Delta L$  and  $L$  would increase by approximately the same factor for each fit. This assumption was verified by a few fits to saturation-corrected pulse-height distributions. Also shown on the plot of Fig. 10 are resolution values for the three gamma-ray pulse-height distributions used for calibration. The pulse-height resolution of the detector for gamma rays appears to be somewhat better than for neutrons which give the same light output.

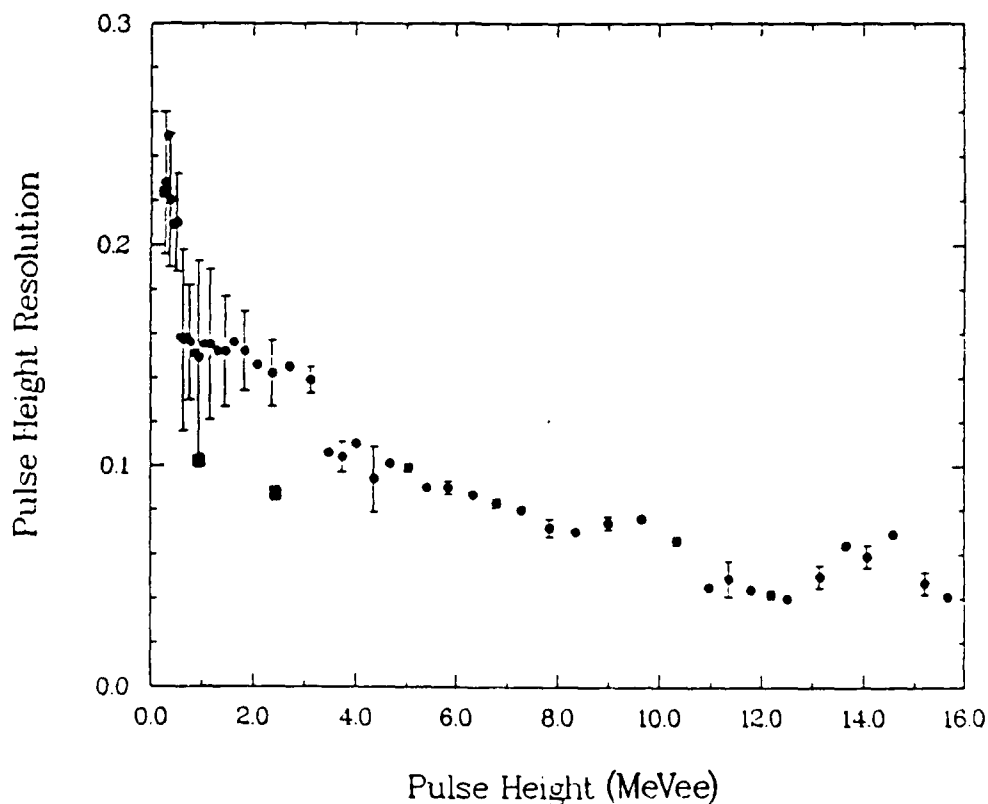


Figure 10. Pulse-height resolution as a function of pulse height for the 5-cm-long by 5-cm-diam BC501 scintillation detector determined from monoenergetic neutron distributions (filled circles) and monoenergetic gamma-ray distributions (filled squares). (Error bars are shown only for every other data point.)

More important than the pulse-height resolution of the detector is the energy resolution  $\Delta E/E$ . The energy resolution along with the unfolding algorithm used determines the overall resolution obtainable for arbitrary neutron energy spectra measured with the BC501 scintillation detector. Figure 11 shows the energy resolution as a function of neutron energy. The energy resolution was obtained from the pulse-height resolution on a point-by-point basis using  $E_n = aL^b$  to describe the relationship between energy and pulse-height. For each energy value  $E_i$ ,  $a$  and  $b$  were determined from  $E_{i-1}$ ,  $E_{i+1}$ ,  $L_{i-1}$ , and  $L_{i+1}$ ; and  $\Delta E_i/E_i$  was determined from  $\Delta E_i/E_i = b\Delta L_i/L_i$ . To check this procedure for determining the energy resolution, a few of the neutron pulse-height distributions were converted to energy distributions using the proton light-output function and their edges fit with a Gaussian-smoothed step function. The energy resolutions obtained from the fits agreed well with the values determined as described above.

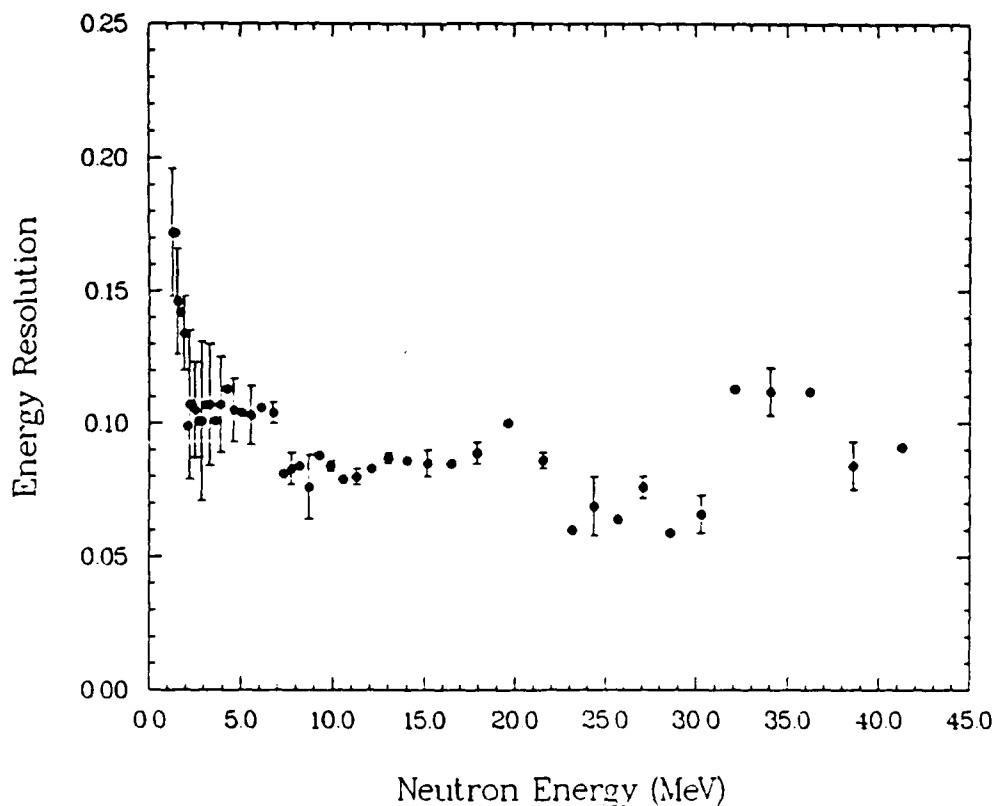


Figure 11. Energy resolution as a function of neutron energy for the 5-cm-long by 5-cm-diam BC501 scintillation detector determined from monoenergetic neutron distributions. (Error bars are shown only for every other data point.)

METHOD OF NORMALIZATION

After calibration of the pulse-height axis and correcting for saturation which occurred above pulse heights of  $\approx 5$  MeVee, the neutron pulse-height distributions were converted to absolute differential efficiencies. The absolute differential efficiency for a given neutron energy is defined as the number of counts per unit pulse height per neutron incident on the cross-sectional area of the top, flat face of the BC501 scintillation detector. For neutron energies  $\leq 30.2$  MeV, conversion to absolute differential efficiencies was accomplished using the technique reported in Ref. 1. The Monte Carlo code O5S (Ref. 16) was used to calculate the absolute differential efficiencies. The calculated differential efficiencies are most accurate at large pulse heights, the large pulse heights being dominantly produced by protons from single (n,p) scattering. Each bin of a calculated pulse-height distribution was redistributed through convolution with a Gaussian function whose FWHM was chosen from the pulse-height resolution curve of our BC501 scintillation detector. The resultant calculated differential efficiencies were plotted with the measured pulse-height distributions. Scale adjustments of the measured pulse-height distributions were made until the calculated and measured distributions matched in the proton-recoil plateau regions, thus converting the measured distributions to absolute differential efficiency curves.

For neutron energies above 30.2 MeV, the O5S code could not be used to generate calculated differential efficiencies. The code failed to run properly for these neutron energies and its output was believed to be unreliable (Ref. 17). Normalization of the measured pulse-height distributions was accomplished using the revised version (Ref. 18) of the neutron detector efficiency code of Stanton (Ref. 19). The areas under the measured pulse-height distribution curves above a cutoff of 1 MeV were made to agree with the calculated integral efficiencies. Cecil, et al (Ref. 18) report that the calculated integral efficiencies of the revised Stanton code agree with a large quantity of experimentally determined efficiencies to within 10 percent.

COMPARISON OF THE BC501 NEUTRON RESPONSE FUNCTIONS TO THE REF. 1 RESPONSE FUNCTIONS

As a check on the saturation correction process and normalization procedure, the absolute differential efficiency curves of the BC501 scintillation detector were compared to the absolute differential efficiency curves for the 4.60-cm-long by 4.65-cm-diam NE213 scintillation detector of Ref. 1. In order to

make the comparison, the NE213 response functions were appropriately scaled to correspond to response functions for a 5-cm-long by 5-cm-diam BC501 scintillator. The scaling corrected for differences in density, composition, scintillator size, and the normalizing cross-sectional area defined by the detector surface upon which the neutrons were incident (see Appendix B). These scaled response functions were then used for the generation of response functions at the neutron energies for which the BC501 response functions were measured. The generation of the NE213 scaled response functions at the appropriate energies was accomplished through two-dimensional interpolation. Figure 12 shows the comparison of the appropriately scaled and interpolated response functions of Ref. 1 to the response functions for our BC501 scintillation detector for four neutron energies spanning the common energy range of 2 to 22 MeV for the two sets of response function measurements. There is very good agreement between the two sets of response functions.

Due to the good agreement between the BC501 response functions and the NE213 response functions of Ref. 1, the NE213 response functions were used to extend the BC501 response functions below a pulse height of  $\approx 0.2$  MeVee, the bias established from the PSD circuitry used during measurement of the neutron pulse-height distributions. The extension of the response functions for neutron energies below 22 MeV was accomplished by generating scaled and interpolated NE213 distributions at pulse heights corresponding to the channel numbers of the neutron two-parameter array of pulse height versus TOF and filling the array below the bias with these distributions. Small additional magnitude corrections ( $\pm 10\%$ ) were sometimes applied to the  $< 0.2$ -MeVee pulse-height sections of the scaled and interpolated NE213 responses to prevent any discontinuities in the resultant BC501 pulse-height distributions near the bias pulse height. The extension of the response functions for neutron energies above 22 MeV was performed by assuming that the shapes of the BC501 responses below a pulse height of  $\approx 0.2$  MeVee were the same as the equivalent region of the 21.5-MeV NE213 response function. Scale adjustments were applied to ensure continuous extension below 0.2 MeVee.

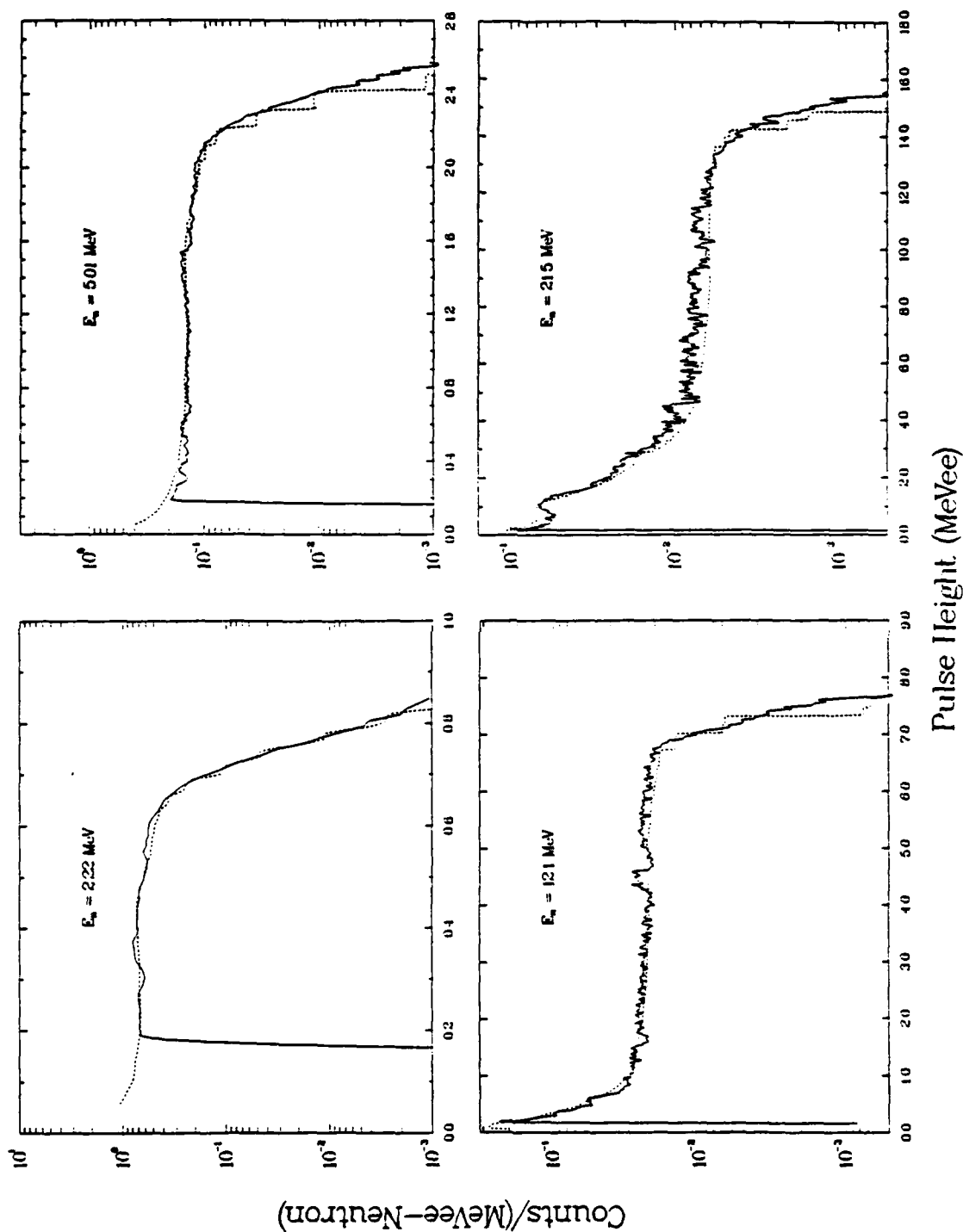


Figure 12. Absolute differential efficiency curves for the 5-cm-long by 5-cm-diam BC501 scintillation detector (solid curves) and the 4.60-cm-long by 4.65-cm-diam NE213 scintillation detector (dashed curves) of Ref. 1 corrected for the differences in density, composition, size, and normalizing cross-sectional area.

## RESULTS AND DISCUSSION

The absolute differential efficiency curves for the 5-cm-long by 5-cm-diam BC501 scintillation detector for the 43 neutron energies between 2 and 41 MeV are shown in Figs. C-1 through C-15 of Appendix C. They are also presented in the table of Appendix D. Appendix D is to be used for construction of a detailed response matrix needed for unfolding a pulse-height distribution acquired with a 5-cm-long by 5-cm-diam BC501 scintillation detector to obtain a neutron energy spectrum. Because of the excellent agreement between the 32 response functions spanning the neutron energy range of 2 to 22 MeV and those of Ref. 1, an error of 5 percent is estimated for the magnitudes of the response curves. This error estimate is a combination of the errors in the Monte Carlo calculations used for normalizing the measured neutron pulse-height distributions and the error in matching the measured to calculated distributions. An error of 2.5 percent is assumed for the magnitudes of the proton-recoil plateaus of the Monte Carlo calculated differential efficiency curves as determined by absolute experimental calibrations (Ref. 1). An error of 4 percent is estimated for matching the proton-recoil plateaus of the measured pulse-height distributions to the calculated proton-recoil plateaus. For the six response functions between neutron energies of 22 and 31 MeV, an error of 11 percent is estimated for the magnitude of the response curves for pulse heights above 0.2 MeVee, a combination of a 5-percent uncertainty in the magnitude of the Monte Carlo calculations and a 10-percent matching uncertainty. No error estimate can be made for pulse heights below 0.2 MeVee since this region of each response function for neutron energies  $> 22$  MeV was an extrapolation of the equivalent region of the 21.5-MeV NE213 response function of Ref. 1. Above a neutron energy of 31 MeV, a reliable estimate of the error in the magnitudes of the response functions is difficult to make. The integral efficiencies for the bias of 0.2 MeVee are estimated to be accurate to within 10 percent. However, above pulse heights of  $\approx 21$  MeVee, there may be large uncertainties in the magnitudes of the response functions due to the saturation of the pulse-height signals during the response function measurements (Ref. 20). Because the area under the response curve above 21 MeVee is a small fraction of the total area, these large uncertainties do not change the error estimate of 10 percent for the integral efficiencies. The authors of Ref. 20 illustrate that the magnitudes of the response functions in the proton-recoil plateau regions are too small by  $\approx 30$  percent for neutron energies  $\leq 36.2$  MeV and factors of 2 to 3 too small for the 38.6- and 41.2-MeV

neutron responses. They argue that because of pulse-height saturation, large pulse-height neutron events were misclassified or lost by the PSD circuitry. All pulse-shape spectra and all pulse-height spectra corresponding to events classified as gamma rays acquired during the neutron response function measurements were examined and no evidence was found to support this argument. However, the simple, analytical calculations performed in Ref. 20 predict proton-recoil plateaus with magnitudes larger than the magnitudes of the large pulse-height regions of the neutron response functions above 31 MeV. As detailed in Ref. 21, if the response functions presented in this report are used for unfolding pulse-height distributions whose magnitudes are decreasing rapidly above  $\approx 21$  MeV, the resultant neutron energy spectra agree within estimated errors to the neutron spectra obtained through unfolding with response functions modified in their recoil-proton plateau regions as outlined in Ref. 20. Disagreeing with modification of only a portion of a response function, the response functions above 31 MeV are presented as measured. However, if they are to be used for unfolding pulse-height distributions which do not decrease rapidly above 21 MeV and are acquired with high statistical accuracy, one may consider using a combination of the experimental and calculated response functions.



## REVIEW AND CONCLUSIONS

Through a combination of TOF measurements and Monte Carlo calculations, the absolute differential efficiencies for a commercial 5-cm-long by 5-cm-diam BC501 scintillation detector were determined at 43 neutron energies in the range of 2 to 41 MeV. The shapes and magnitudes of the BC501 neutron response functions in the neutron energy range of 2 to 22 MeV agree well with the shapes and magnitudes of the standard NE213 scintillator responses (Ref. 1) when corrected for density, composition, scintillator size, and cross-sectional area differences. Also, comparison (Ref. 22) of the quality of neutron/gamma-ray discrimination obtainable with two identical cells filled with NE213 and BC501 scintillating liquids shows that their PSD properties are very similar. Therefore, similarly constructed NE213 and BC501 scintillation detectors are equivalent in their use for neutron spectroscopy measurements. The measurements presented in this report allow construction of a detailed response matrix to be used for pulse-height unfolding of neutron distributions up to energies of 41 MeV. With simple scale adjustments to correct for density and composition differences, these BC501 neutron response functions can also be used for unfolding pulse-height distributions acquired with a 5-cm-long by 5-cm-diam NE213 scintillation detector.

## REFERENCES

1. Verbinski, V. V., W. R. Burrus, T. A. Love, W. Zobel, and N. W. Hill, "Calibration of an Organic Scintillator for Neutron Spectrometry," Nucl. Instr. Meth., 65, 8 (1968).
2. Burrus, W. R., and V. V. Verbinski, "Fast-Neutron Spectroscopy with Thick Organic Scintillators," Nucl. Instr. Meth., 67, 181 (1969).
3. Pieroni, N., D. Rusch, and E. Wattecamps, "Measurement of Time-Dependent Fast Neutron Spectra with an NE213 Scintillator," Nucl. Instr. Meth., 115, 317 (1974).
4. Morgan, G. L., T. A. Love, and F. G. Perey, "An Experimental System for Providing Data to Test Evaluated Secondary Neutron and Gamma-Ray-Production Cross Sections Over the Incident Neutron Energy Range from 1 to 20 MeV," Nucl. Instr. Meth., 128, 125 (1975).
5. Morgan, G. L., and A. C. England, "Measurement of Neutron Flux from a Tokamak Plasma Device," Nucl. Instr. Meth., 129, 1 (1975).
6. Dickens, J. K., N. W. Hill, F. S. Hou, J. W. McConnell, R. R. Spencer, and F. Y. Tsang, An NE213-Scintillator-Based Neutron Detection System for Diagnostic Measurements of Energy Spectra for Neutrons Having Energies > 0.8 MeV Created During Plasma Operations at the Princeton Tokamak Fusion Test Reactor, Oak Ridge National Laboratory, Oak Ridge, Tenn, ORNL/TM-9561 (1985).
7. Nordell, B., "Measurement of Photoneutron Energy Spectra from Tin, Lead and Uranium Using an NE-213 Neutron Spectrometer," Nucl. Instr. Meth., 224, 547 (1984).
8. Erduran, M. N., and R. B. Galloway, "Neutron Elastic and Inelastic Differential Scattering Cross-Sections by Proton Recoil Spectrum Unfolding," Nucl. Instr. Meth., A238, 83 (1985).
9. Nakamura, T., M. Yoshida, and K. Shin, "Spectral Measurements of Neutrons and Photons from Thick Targets of C, Fe, Cu and Pb by 52 MeV Protons," Nucl. Instr. Meth., 151, 493 (1978).
10. Premium Plastic and Liquid Scintillators, Bicron Corporation, 12345 Kinsman Rd., Newbury, Ohio 44065 (1986).
11. "NE213 Liquid Scintillator for Neutron Spectrometry Using Pulse Shape Discrimination," Bulletin 404, Nuclear Enterprises Ltd. Sighthill, Edinburgh EH11 4BY, Scotland (1979).
12. Perkins, L. J., The Design and Development of a Miniature Fast-Neutron Scintillation Spectrometer and its Application to the Fusion Neutronics of a Lithium Fluoride Integral Benchmark Experiment, Ph.D. Thesis, University of Birmingham, Birmingham B15 2TT, England (1978).
13. Flynn, K. F., L. E. Glendenin, E. P. Steinberg, and P. M. Wright, "Pulse Height-Energy Relations for Electrons and Alpha Particles in a Liquid Scintillator," Nucl. Instr. Meth., 27, 13 (1964).

REFERENCES (Concluded)

14. Dietz, G., and H. Klein, "Gamma Calibration of NE213 Scintillation Counters," Nucl. Instr. Meth., 193, 549 (1982).
15. James, F. and M. Roos, "MINUIT--A System for Function Minimization and Analysis of the Parameter Errors and Correlations," Computer Physics Communications, 10, 343 (1975).
16. Textor, R. E. and V. V. Verbinski, O5S: A Monte Carlo Code for Calculating Pulse Height Distributions Due to Monoenergetic Neutrons Incident on Organic Scintillators, Oak Ridge National Laboratory, Oak Ridge, Tenn, ORNL-4160 (1968).
17. Dickens, J. K., Oak Ridge National Laboratory, private communication.
18. Cecil, R. A., B. D. Anderson and R. Madey, "Improved Predictions of Neutron Detection Efficiency for Hydrocarbon Scintillators from 1 MeV to about 300 MeV," Nucl. Instr. Meth., 161, 439 (1979).
19. Stanton, N. R., Ohio State University Report COO-1545-92 (1971).
20. Reed, J. H., and V. V. Verbinski, Measured Neutron and Discrete Gamma-Ray Spectra from Thick Targets Bombarded by 50-MeV Protons, Radiation Technologies, Escondido, Calif. RT-87TRW1-F (1987).
21. Kiziah, R. R., D. S. Ek, J. B. Martin, M. P. Snell, and W. G. Wilson, Energy and Angular Distributions of Secondary Neutrons from Targets Bombarded by 50-MeV Protons, AFWL-TR-87-63, Air Force Weapons Laboratory, Kirtland AFB, N. Mex., April 1988.
22. Goulding, C. A., A. A. Robba, and E. R. Shunk, Comparison of the Scintillators BC501 and NL213, Los Alamos National Laboratory, Los Alamos, N. Mex., LA-N2TN-87-201 (1987).

## APPENDIX A

DETERMINING THE PROTON LIGHT-OUTPUT FUNCTION,  $L(E_p)$ ,  
FROM MEASURED MONOENERGETIC NEUTRON  
PULSE-HEIGHT DISTRIBUTIONS

Since the BC501 liquid organic scintillator consists only of hydrogen and carbon, a neutron interacts with the scintillator through elastic scattering from hydrogen nuclei and elastic and nonelastic scattering from carbon nuclei. Assuming no interaction with the carbon nuclei and that the neutron scatters only once from the hydrogen nuclei, one can derive an analytical expression for the energy distribution of recoiling protons which is essentially the response function of the scintillator. Defining  $P(E_p)dE_p$  to be the probability that the recoiling proton has an energy within  $dE_p$  centered about  $E_p$ ,

$$P(E_p)dE_p = P(\theta)d\theta \quad (A-1)$$

where  $P(\theta)d\theta$  is the probability that the neutron was scattered into the angular range  $d\theta$  centered about  $\theta$ .  $E_p$  is the recoil proton kinetic energy in the laboratory coordinate system and  $\theta$  is the scattering angle of the neutron in the center-of-mass coordinate system.  $P(\theta)d\theta$  is given by

$$P(\theta)d\theta = 2\pi\sin\theta d\theta \sigma(\theta)/\sigma_T \quad (A-2)$$

where  $\sigma(\theta)$  is the differential elastic scattering cross section in the center-of-mass system and  $\sigma_T$  is the total scattering cross section. Combining Eqs. A-1 and A-2,

$$P(E_p) = 2\pi\sin\theta \left[ \sigma(\theta)/\sigma_T \right] \left[ d\theta/dE_p \right] \quad (A-3)$$

From conservation of energy and momentum (nonrelativistic kinematics)

$$E_p = E_n(1 - \cos\theta)/2 \quad (A-4)$$

where  $E_n$  is the incident neutron kinetic energy in the laboratory coordinate system. Using Eq. A-4 to solve for  $d\theta/dE_p$  and substituting the result into Eq. A-3,

$$P(E_p) = 4\pi [\sigma(\theta)/\sigma_T] (1/E_n) \quad (A-5)$$

For neutrons with kinetic energies < 10 MeV, the elastic scattering process from hydrogen nuclei is isotropic in the center-of-mass system. Above kinetic energies of 10 MeV, the elastic scattering process is not isotropic but will be taken as isotropic for purposes of this derivation. Therefore,  $\sigma(\theta) = \sigma_T/4\pi$  and

$$P(E_p) = 1/E_n \quad (A-6)$$

The energy distribution of recoil protons is uniform, extending from zero kinetic energy to the incident neutron kinetic energy.

The response function of the scintillator to monoenergetic neutrons is the distribution of light pulses as a result of the recoiling protons. Assuming a linear relationship between light output,  $L_p$ , and proton energy deposition in the scintillator,

$$P(L_p) = C/E_n \quad (A-7)$$

where C is a constant. Thus, the response function or pulse-height distribution of the scintillator to a source of monoenergetic neutrons is a rectangle. Folding a Gaussian function with Eq. A-7, to approximate finite resolution effects of the scintillation detector, yields

$$R(L) = \{S_o/2\} \left\{ 1 - \operatorname{erf} \left[ (L - L_o) / (\sqrt{2}\sigma) \right] \right\} \quad (A-8)$$

where  $S_o = C/E_n$ ,  $L_o$  is the light output corresponding to the maximum recoiling proton kinetic energy deposition ( $E_p = E_n$ ), and erf is the error function. From Eq. A-8, when  $L = L_o$ , the error function is zero and the response curve  $R(L)$  equals one-half of its maximum value  $S_o$ . Fitting Eq. A-8 to the edges of a series of pulse-height distributions for monoenergetic neutrons allows determination of the light-output function,  $L(E_p)$ , for the scintillation detector.  $L(E_p)$  consists of the series of  $L_o$ 's determined from the fits.

Care must be exercised in using Eq. A-8 in fitting the edges of monoenergetic neutron pulse-height distributions to determine  $L(E_p)$ . Only a small range of

the pulse-height distribution about  $L = L_0$  is represented by Eq. A-8 because of the simplifying assumptions used in its derivation. For example, the light output from the scintillator does not increase linearly with the recoiling proton energy deposition. However, the light-output function can be approximated by a piecewise continuous function consisting of a set of linear functions with each one valid over a small range of light output. Another distortion of the ideal pulse-height distribution represented by Eq. A-8 is the edge effect. The highest-energy recoiling protons may escape from the scintillator before depositing all of their kinetic energies. Thus, events in the ideal pulse-height distribution are shifted from high pulse heights to low pulse heights. However, at the higher neutron energies, the edge effect is partially compensated for by the nonisotropy of the neutron elastic scattering process. Lastly, multiple scattering of neutrons from hydrogen nuclei and scattering from carbon nuclei distort the ideal pulse-height distribution. Nonetheless, as the four graphs of Fig. 7 show, when applied with care Eq. A-8 is a useful representation of the edge of a monoenergetic neutron pulse-height distribution for a wide range of neutron energies.

## APPENDIX B

METHOD OF CONVERTING RESPONSE FUNCTIONS OF A 4.60-CM-LONG BY  
4.65-CM-DIAM NE213 SCINTILLATION DETECTOR TO RESPONSE FUNCTIONS  
OF A 5-CM-LONG BY 5-CM-DIAM BC501 SCINTILLATION DETECTOR

Since the NE213 scintillation detector of Ref. 1 is very similar to a 5-cm-long by 5-cm-diam BC501 scintillation detector, conversion of the NE213 response functions to BC501 response functions consists only of a scale adjustment. The appropriate scaling factor can be estimated from a simple analytical expression for the integral efficiency of an organic scintillator. The integral efficiency for a given energy bias  $E_B$  is the area under the absolute differential efficiency curve above the bias. If the bias is chosen appropriately, the pulse-height distribution above the bias is only a result of recoiling protons. However, these recoiling protons can result from single elastic scattering of neutrons from hydrogen nuclei (n-H), double elastic scattering of neutrons from hydrogen nuclei (n-H + n-H), and elastic or inelastic scattering of neutrons from carbon nuclei followed by elastic scattering from hydrogen nuclei (n-C + n-H), and other higher-order scattering processes. Considering only n-H, n-H + n-H, and n-C + n-H scattering processes, one can derive an analytical expression for the integral efficiency of an organic scintillator for a bias  $E_B$  such that all events above the bias are due to recoiling protons.

The absolute differential efficiency curve is the number of pulse-height events per incident neutron per unit pulse height. Therefore, the integral efficiency for a bias  $E_B$  is a sum of three products (one for each scattering process), each product consisting of the probability that one neutron will produce a resultant recoiling proton times the probability that the recoiling proton will have a kinetic energy between  $E_B$  and  $E_n$ , where  $E_n$  is the incident neutron kinetic energy. From Eq. A-5, the probability that a recoiling proton will have a kinetic energy between  $E_B$  and  $E_n$  is

$$P_{E_p} = \int_{E_B}^{E_n} 4\pi \left[ \sigma(\theta) / \sigma_T \right] \left( 1/E_n \right) dE_p$$

For neutrons with kinetic energies  $\leq 10$  MeV,

$$\sigma(\theta) = \sigma_T/4\pi$$

For neutrons with kinetic energies  $> 10$  MeV,

$$\sigma(\theta) = (\sigma_T/4) \left\{ \left[ 1 + b \cos^2 \theta \right] / \left[ 1 + (1/3)b \right] \right\}$$

where

$$b = 2 \left( E_n/90 \right)^2$$

and

$$\cos \theta = 1 - 2E_p/E_n$$

The expression for the probability that one neutron will produce a resultant recoiling proton depends upon the scattering process. As an example, for the n-H scattering process, this expression is derived as follows. The probability that a neutron will travel a distance  $x$  into a scintillator without having an interaction is  $\exp\left[-\Sigma_T(E_n)x\right]$  where  $\Sigma_T(E_n) = \Sigma_H(E_n) + \Sigma_C(E_n) = n_H\sigma_H(E_n) + n_C\sigma_C(E_n)$ , where  $n_H$  and  $n_C$  are the number densities of the hydrogen and carbon nuclei, and  $\sigma_H$  and  $\sigma_C$  are the total scattering cross sections of a neutron from hydrogen and carbon nuclei, respectively. The probability that the neutron will scatter from a hydrogen nucleus in the distance  $dx$  centered about  $x$  is  $\Sigma_H(E_n)dx$ . Thus the probability that one neutron will produce a resultant recoiling proton in a scintillator of thickness  $t$  is

$$P_p = \int_0^t \Sigma_H(E_n) \exp\left[-\Sigma_T(E_n)x\right] dx$$

The integral efficiency is merely a sum of products:  $P_{Ep}P_p(n-H) + P_{Ep}P_p(n-H + n-H) + P_{Ep}P_p(n-C + n-H)$ .

For neutrons with kinetic energies  $\leq 10$  MeV, an expression for the integral efficiency for a bias  $E_B$  is



integral efficiency (bias  $E_B$ ,  $E_n \leq 10$  MeV) -

$$\begin{aligned}
 & \left[ \left( \frac{E_n - E_B}{E_n} \right) \left[ \frac{\Sigma_H(E_n)}{\Sigma_T(E_n)} \right] \left\{ 1 - \exp \left[ -\Sigma_T(E_n) t \right] \right\} \right. \\
 & + \left( \frac{E_B}{E_n} \right) \left[ \left( \frac{E_n - E_B}{E_n - E_B/2} \right) \left[ \frac{\Sigma_H(E_n)}{\Sigma_T(E_n)} \right] \right. \\
 & \times \left[ \frac{\Sigma_H(E_n - E_B/2)}{\Sigma_T(E_n - E_B/2)} \right] \left\{ 1 - \exp \left[ -\Sigma_T(E_n) t \right] \right\} \\
 & \times \left[ 1 - \exp \left[ -\Sigma_T(E_n - E_B/2) t/2 \right] \right] \\
 & + F \left[ \left( \frac{0.86E_n - E_B}{0.86E_n} \right) \left[ \frac{\Sigma_C(E_n)}{\Sigma_T(E_n)} \right] \right. \\
 & \times \left[ \frac{\Sigma_H(0.86E_n)}{\Sigma_T(0.86E_n)} \right] \left\{ 1 - \exp \left[ -\Sigma_T(E_n) t \right] \right\} \\
 & \times \left. \left\{ 1 - \exp \left[ -\Sigma_T(0.86E_n) 4V/S \right] \right\} \right] \quad (B-1)
 \end{aligned}$$

where  $V$  is the volume of the scintillator,  $S$  is the surface area, and  $F = 1$  if  $E_B \leq 0.72E_n$  or  $F = (E_n - E_B)/0.28E_n$  if  $E_B > 0.72E_n$ . The three terms of Eq. B-1 are the integral efficiency contributions from the n-H, n-H + n-H, and n-C + n-H scattering processes. The assumptions used in deriving the second and third terms were taken from Refs. B-1 and B-2. In the n-H + n-H scattering process, the first n-H scattering produces a recoiling proton with kinetic energy uniformly distributed between 0 and  $E_B$ . In the second n-H scattering, any recoiling protons produced with kinetic energies above  $E_B/2$  add to the first recoiling proton to produce a resultant recoiling proton with an energy greater than  $E_B$ . The effective scintillator thickness for the second scattering is  $t/2$ , and the effective neutron energy after the first scattering is  $E_n - E_B/2$ . In the n-C + n-H scattering process, the n-C scattering produces a recoiling carbon nucleus with kinetic energy uniformly distributed between 0 and  $0.28E_n$ . The effective scintillator thickness for the n-H scattering is  $4V/S$ , the mean chord length in the scintillator, and the effective neutron energy after the n-C scattering is  $0.86E_n$ .  $F$  accounts for those cases in which the bias is so high that some or all of the neutrons do not have enough kinetic energy to produce recoiling protons above the bias after having scattered from carbon.

An expression similar to Eq. B-1 can be derived for the integral efficiency for neutrons with kinetic energies  $> 10$  MeV. Using the same assumptions,

ignoring the n-H + n-H scattering process, and accounting for the nonisotropy of the n-H scattering,

integral efficiency (bias  $E_B$ ,  $E_n > 10$  MeV) -

$$\begin{aligned}
 & (1/E_n) \left[ \Sigma_H(E_n)/\Sigma_T(E_n) \right] \left\{ 1 - \exp \left[ -\Sigma_T(E_n)t \right] \right\} \\
 & \times \left\{ \left[ E_n - E_B + (2/3)(E_n/90)^2 \right] \left[ E_n - E_B \left( 3 - 6E_B/E_n + 4(E_B/E_n)^2 \right) \right] \right\} \\
 & / \left[ 1 + (2/3) \left( E_n/90 \right)^2 \right] \\
 & + F \left[ \Sigma_C(E_n)/\Sigma_T(E_n) \right] \left\{ 1 - \exp \left[ -\Sigma_T(E_n)t \right] \right\} \left[ \Sigma_H(0.86E_n)/\Sigma_T(0.86E_n) \right] \\
 & \times \left[ 1/0.86E_n \right] \left\{ \left[ 0.86E_n - E_B + (2/3) \left( 0.86E_n/90 \right)^2 \right] \left[ 0.86E_n \right. \right. \\
 & \left. \left. - E_B \left( 3 - 6E_B/0.86E_n + 4 \left( E_B/0.86E_n \right)^2 \right) \right] \right\} \\
 & / \left[ 1 + (2/3) \left( 0.86E_n/90 \right)^2 \right] \\
 & \times \left[ 1 - \exp \left[ -\Sigma_T(0.86E_n)4V/S \right] \right] \tag{B-2}
 \end{aligned}$$

The scaling factors for converting the 4.60-cm-long by 4.65-cm-diam NE213 response functions to 5-cm-long by 5-cm-diam BC501 response functions were calculated using the ratios of the integral efficiencies for the BC501 scintillator to the integral efficiencies for the NE213 scintillator. Both efficiencies were computed at the same bias  $E_B$ . For the NE213 scintillator, the thickness used in Eqs. B-1 and B-2 was taken as 3.65 cm, which is the mean thickness of the scintillator for neutrons incident on the curved side (Ref. B-1). The bias  $E_B$  was varied for each ratio calculation and was selected as the value giving the best agreement between calculated and measured NE213 integral efficiencies. The measured efficiencies were taken from Ref. 1. With optimum selection of the  $E_B$ 's, Eqs. B-1 and B-2 yielded NE213 integral efficiencies within 5 percent of the measured efficiencies of Ref. 1.

REFERENCES

- B-1. Drosch, M., "Accurate Measurement of the Counting Efficiency of a NE213 Neutron Detector Between 2 and 26 MeV," Nucl. Instr. Meth., 105, 573 (1972).
- B-2. Fowler, J. L., J. A. Cookson, M. Hussain, R. B. Schwartz, M. T. Swinhoe, C. Wise, and C. A. Uttley, "Efficiency Calibration of Scintillation Detectors in the Neutron Energy Range 1.5 - 25 MeV by the Associated Particle Technique," Nucl. Instr. Meth., 175, 449 (1980).

## APPENDIX C

ABSOLUTE DIFFERENTIAL EFFICIENCY CURVES FOR THE 5-CM-LONG  
BY 5-CM-DIAM BC501 SCINTILLATION DETECTOR FOR  
NEUTRON ENERGIES BETWEEN 2 AND 41 MeV

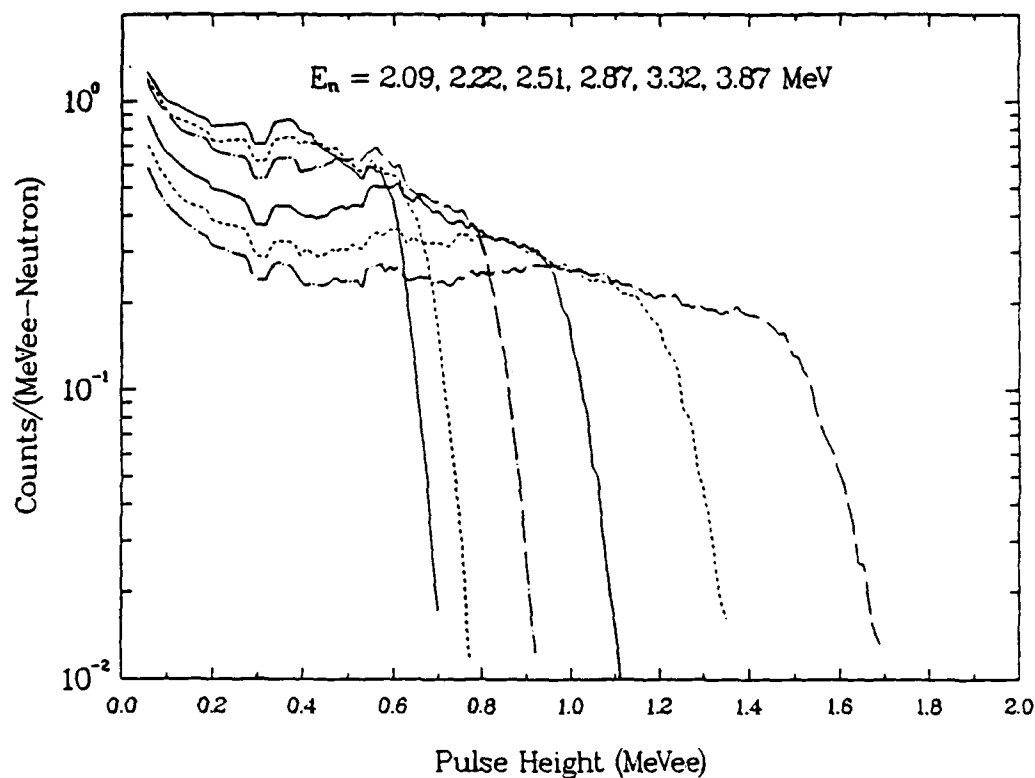


Figure C-1. Absolute differential efficiency curves for the 5-cm-long by 5-cm-diam BC501 scintillation detector for neutron energies of 2.09, 2.22, 2.51, 2.87, 3.32, and 3.87 MeV.

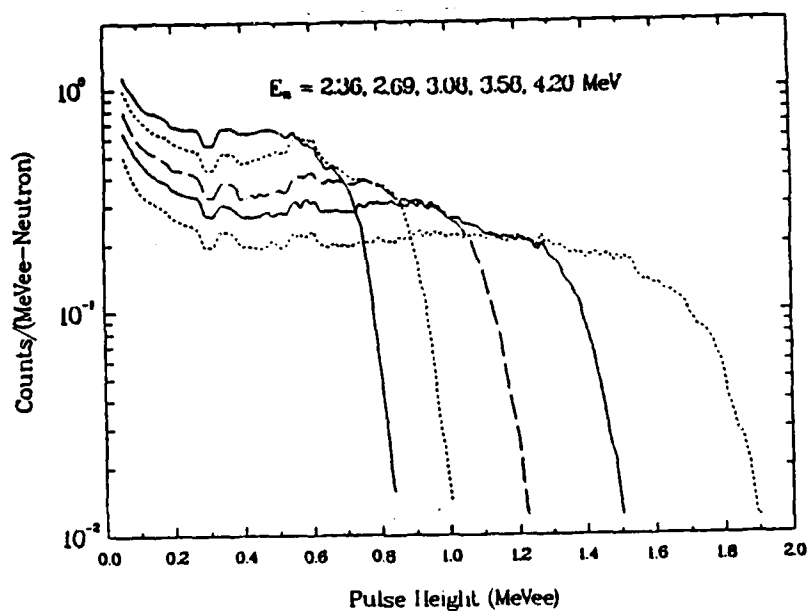


Figure C-2. Absolute differential efficiency curves for the 5-cm-long by 5-cm-diam BC501 scintillation detector for neutron energies of 2.36, 2.69, 3.08, 3.58, and 4.20 MeV.

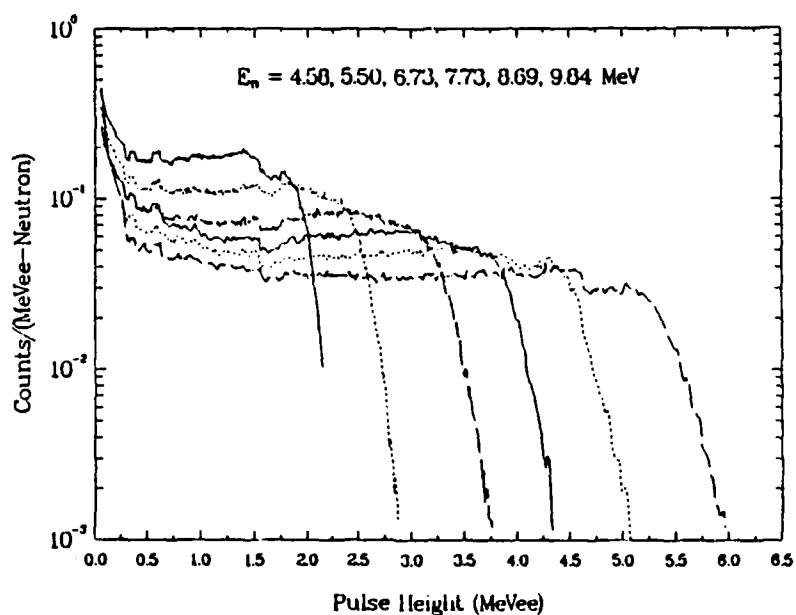


Figure C-3. Absolute differential efficiency curves for the 5-cm-long by 5-cm-diam BC501 scintillation detector for neutron energies of 4.58, 5.50, 6.73, 7.73, 8.69, and 9.84 MeV.

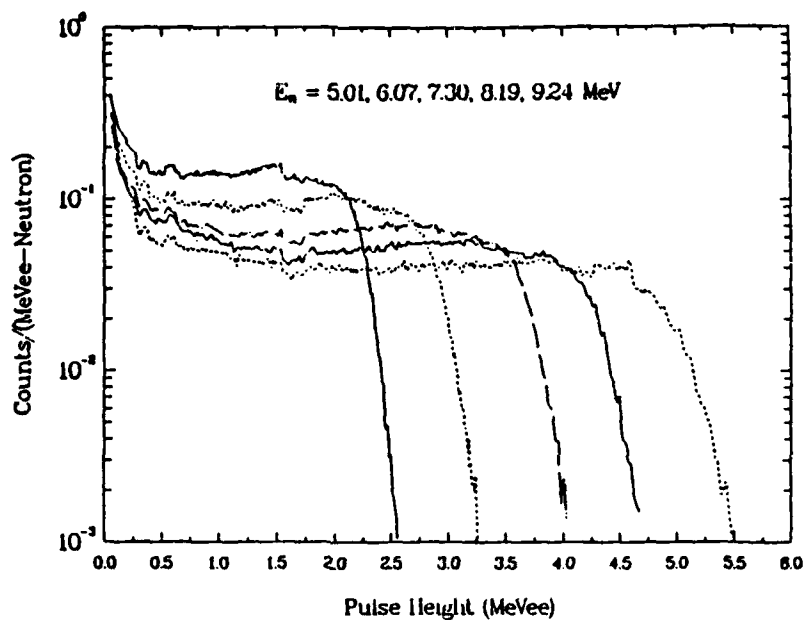


Figure C-4. Absolute differential efficiency curves for the 5-cm-long by 5-cm-diam BC501 scintillation detector for neutron energies of 5.01, 6.07, 7.30, 8.19, and 9.24 MeV.

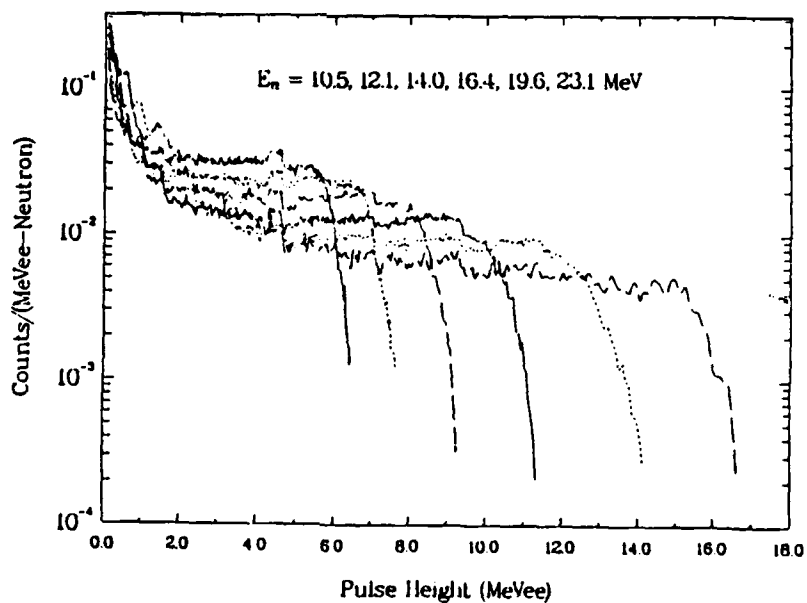


Figure C-5. Absolute differential efficiency curves for the 5-cm-long by 5-cm-diam BC501 scintillation detector for neutron energies of 10.5, 12.1, 14.0, 16.4, 19.6, and 23.1 MeV.

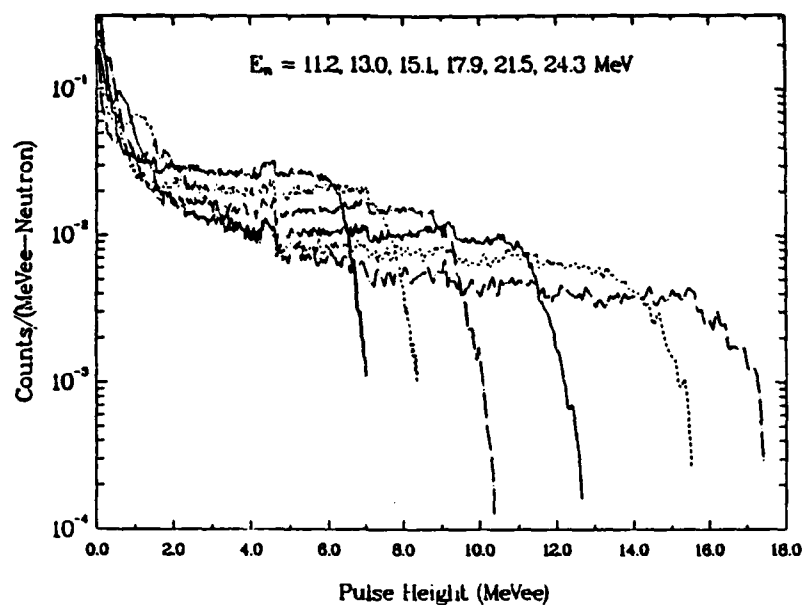


Figure C-6. Absolute differential efficiency curves for the 5-cm-long by 5-cm-diam BC501 scintillation detector for neutron energies of 11.2, 13.0, 15.1, 17.9, 21.5, and 24.3 MeV.

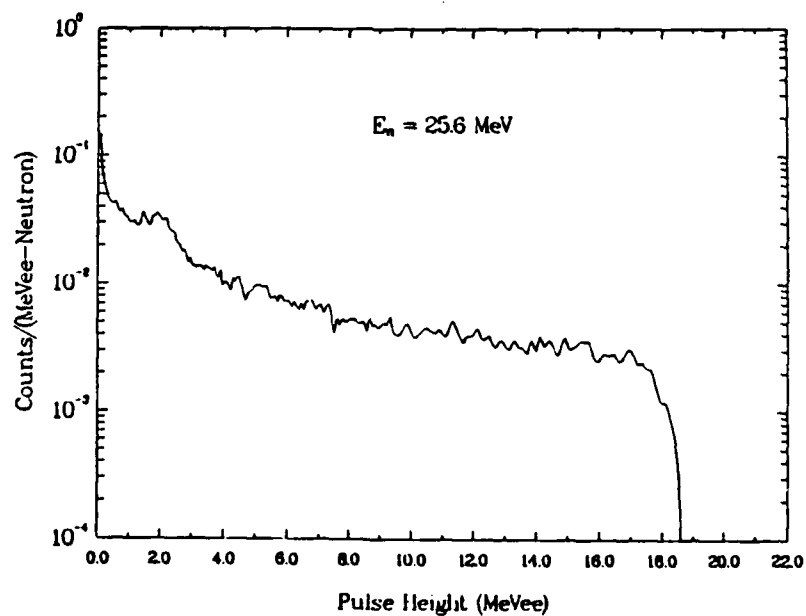


Figure C-7. Absolute differential efficiency curves for the 5-cm-long by 5-cm-diam BC501 scintillation detector for a neutron energy of 25.6 MeV.

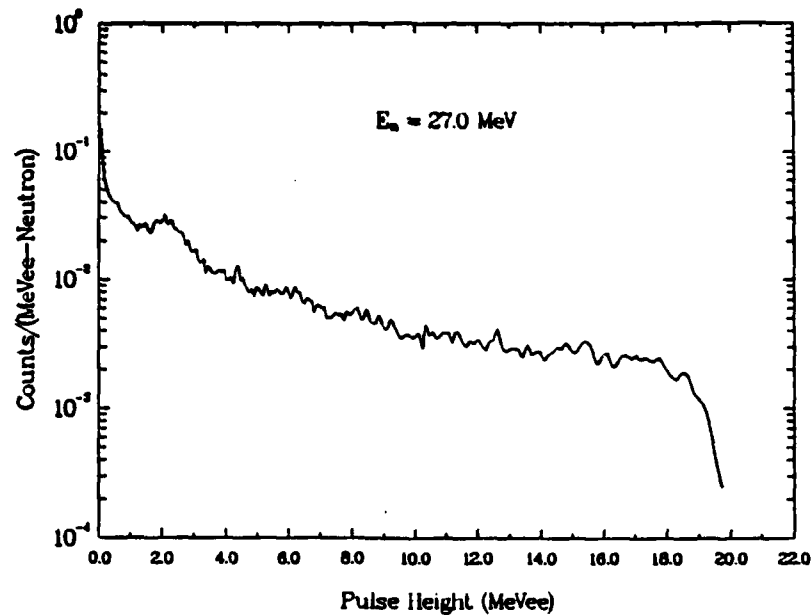


Figure C-8. Absolute differential efficiency curve for the 5-cm-long by 5-cm-diam BC501 scintillation detector for a neutron energy of 27.0 MeV.

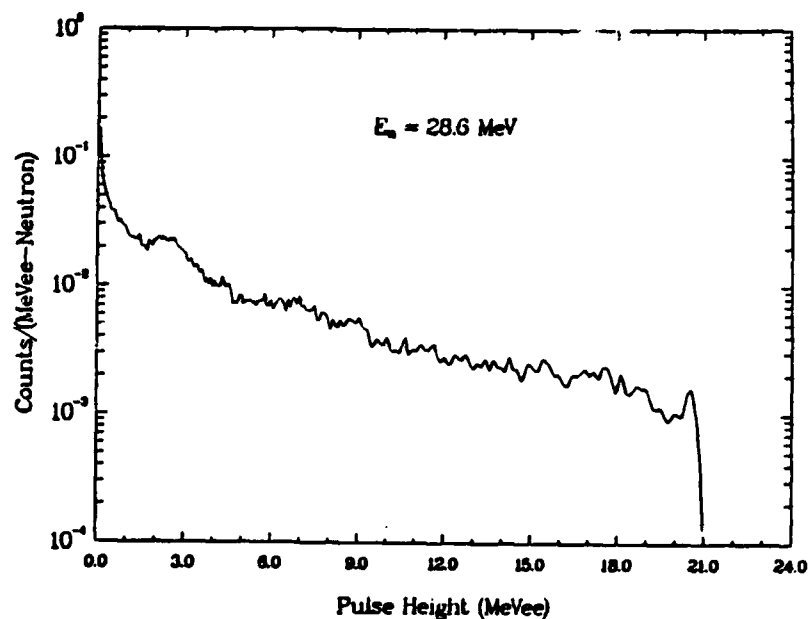


Figure C-9. Absolute differential efficiency curve for the 5-cm-long by 5-cm-diam BC501 scintillation detector for a neutron energy of 28.6 MeV.



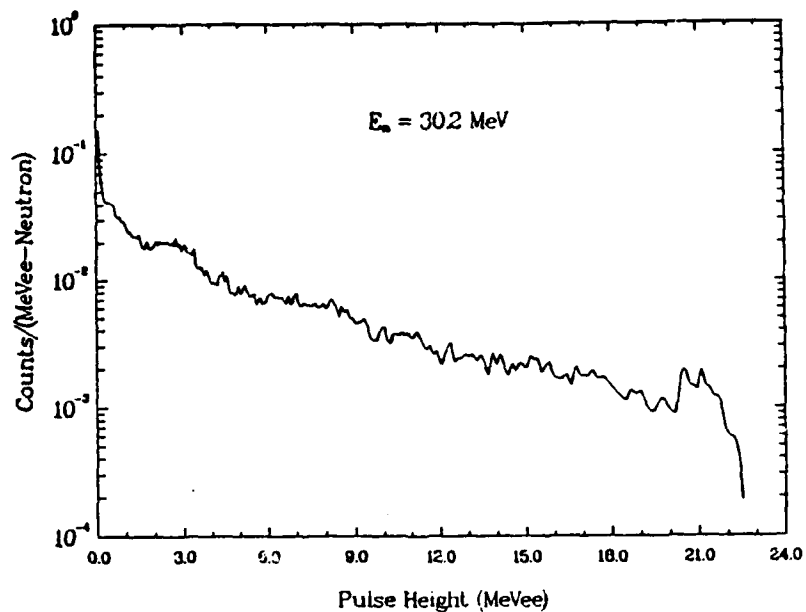


Figure C-10. Absolute differential efficiency curves for the 5-cm-long by 5-cm-diam BC501 scintillation detector for a neutron energy of 30.2 MeV.

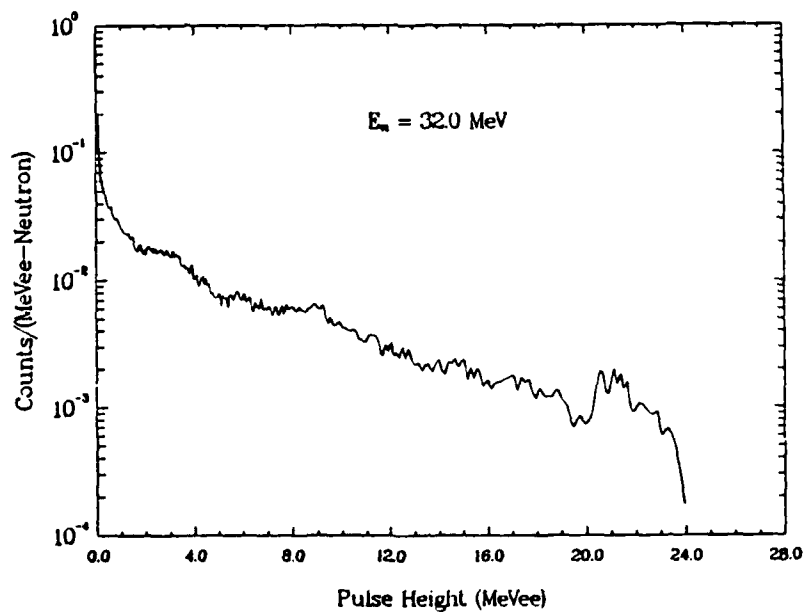


Figure C-11. Absolute differential efficiency curves for the 5-cm-long by 5-cm-diam BC501 scintillation detector for a neutron energy of 32.0 MeV.

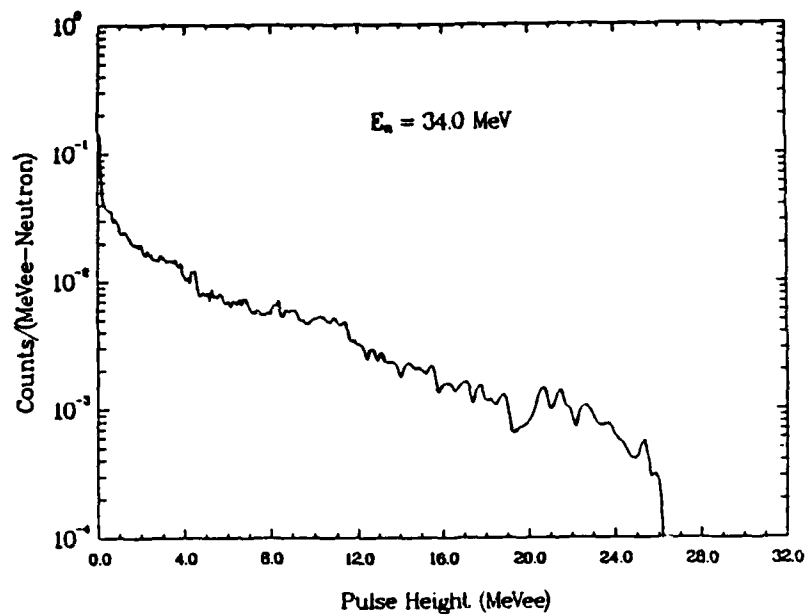


Figure C-12. Absolute differential efficiency curves for the 5-cm-long by 5-cm-diam BC501 scintillation detector for a neutron energy of 34.0 MeV.

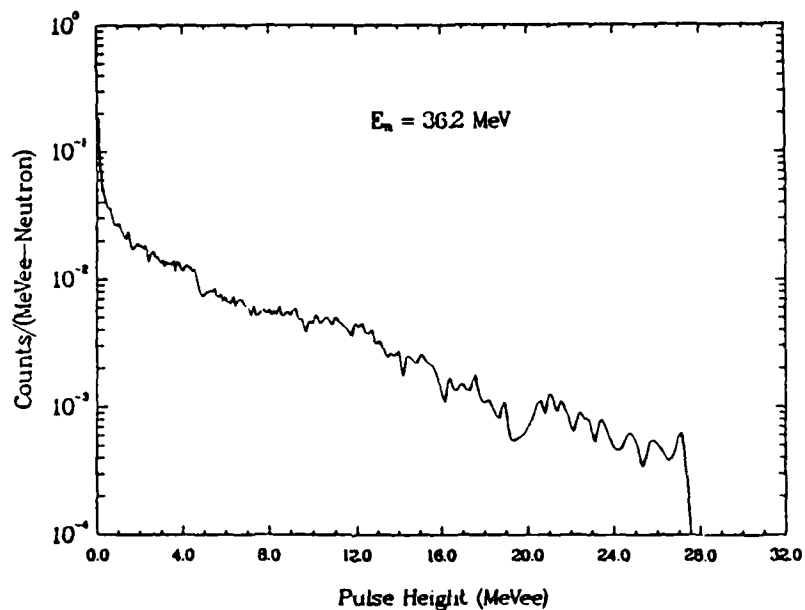


Figure C-13. Absolute differential efficiency curves for the 5-cm-long by 5-cm-diam BC501 scintillation detector for a neutron energy of 36.2 MeV.

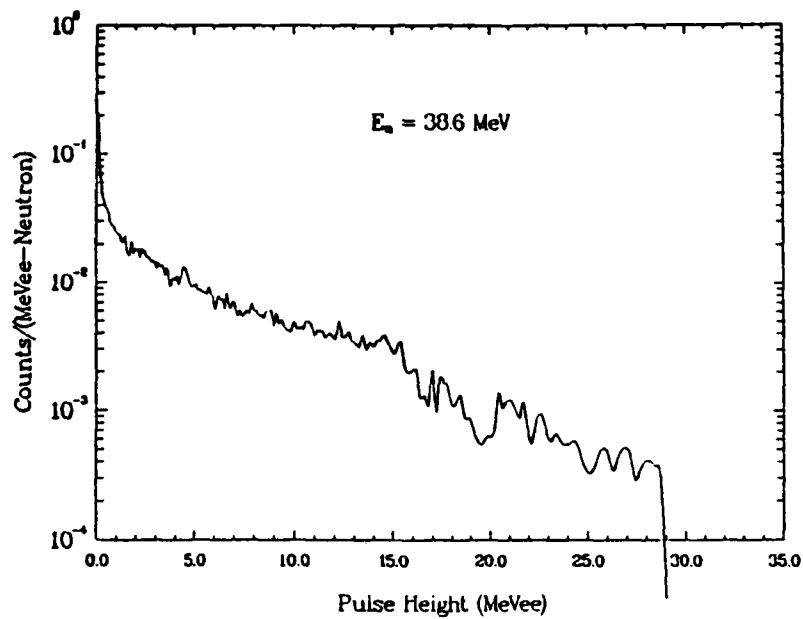


Figure C-14. Absolute differential efficiency curves for the 5-cm-long by 5-cm-diam BC501 scintillation detector for a neutron energy of 38.6 MeV.

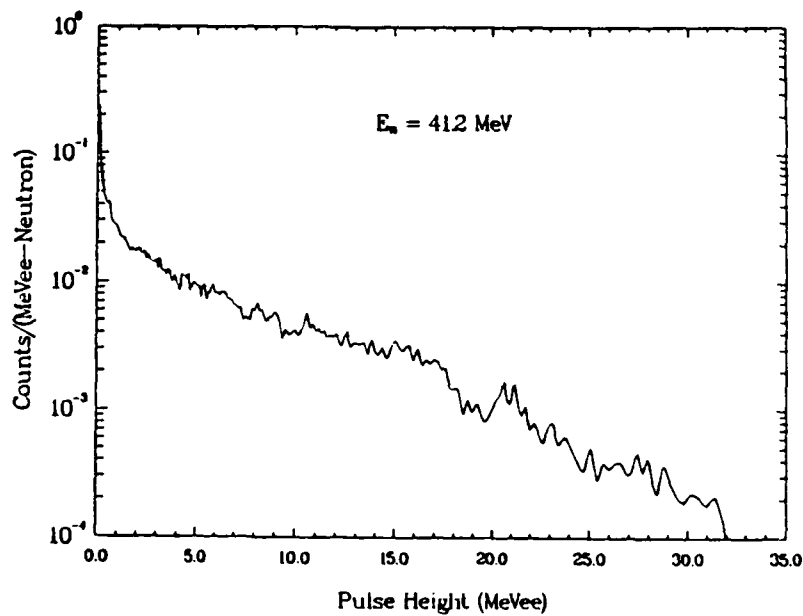


Figure C-15. Absolute differential efficiency curves for the 5-cm-long by 5-cm-diam BC501 scintillation detector for a neutron energy of 41.2 MeV.

## APPENDIX D

TABULATION OF ABSOLUTE DIFFERENTIAL EFFICIENCY VERSUS  
PULSE HEIGHT OF A 5-CM-LONG BY 5-CM-DIAM CYLINDRICAL  
BC501 SCINTILLATION DETECTOR FOR MONOENERGETIC NEUTRONS  
INCIDENT ON THE TOP, FLAT FACE OF THE SCINTILLATOR

Pulse Height (MeVee)	Neutron Energy				
	2.09 MeV	2.22 MeV	2.36 MeV	2.51 MeV	2.69 MeV
0.057 - 0.067	1.19860	1.12582	1.06092	1.06985	0.91573
0.067 - 0.077	1.12609	1.07097	1.01142	1.00219	0.84785
0.077 - 0.087	1.05845	1.00369	0.96519	0.96105	0.80027
0.087 - 0.097	1.01195	0.93847	0.90903	0.91969	0.77096
0.097 - 0.107	0.98802	0.89576	0.85972	0.87617	0.74101
0.107 - 0.117	0.97447	0.87343	0.82295	0.83655	0.71297
0.117 - 0.127	0.96165	0.86231	0.80201	0.80266	0.68645
0.127 - 0.137	0.94471	0.85249	0.78976	0.78099	0.66289
0.137 - 0.149	0.92135	0.83837	0.78141	0.76790	0.64162
0.149 - 0.161	0.89867	0.82089	0.77003	0.75883	0.62954
0.161 - 0.174	0.87967	0.79952	0.75534	0.74893	0.62118
0.174 - 0.189	0.86207	0.77715	0.73145	0.73110	0.60967
0.189 - 0.205	0.83004	0.74056	0.69091	0.69006	0.58037
0.205 - 0.222	0.82509	0.72545	0.67333	0.66479	0.56047
0.222 - 0.240	0.82707	0.72833	0.66304	0.65370	0.54433
0.240 - 0.260	0.83038	0.73217	0.66381	0.64282	0.53366
0.260 - 0.282	0.83208	0.72836	0.65918	0.63449	0.52004
0.282 - 0.305	0.72166	0.63157	0.57026	0.54722	0.44497
0.305 - 0.331	0.73454	0.63851	0.57735	0.55189	0.44737
0.331 - 0.358	0.85740	0.74253	0.66618	0.63609	0.51320
0.358 - 0.388	0.85281	0.74970	0.66482	0.62635	0.50424
0.388 - 0.421	0.77228	0.71914	0.63599	0.58045	0.47245
0.421 - 0.456	0.68740	0.69760	0.64265	0.60005	0.48589
0.456 - 0.494	0.62539	0.66287	0.65482	0.62801	0.51145
0.494 - 0.535	0.56061	0.58480	0.62225	0.62641	0.52508
0.535 - 0.579	0.56118	0.58784	0.60018	0.66263	0.59223
0.579 - 0.627	0.36195	0.52488	0.53529	0.57926	0.57248
0.627 - 0.680	0.09205	0.34069	0.43777	0.47562	0.46102
0.680 - 0.736	0.01075	0.11222	0.33586	0.43273	0.40576
0.736 - 0.798	0.00142	0.01588	0.14184	0.37364	0.38022
0.798 - 0.864	0.00030	0.00161	0.01919	0.17559	0.33882
0.864 - 0.936	0.00000	0.00000	0.00103	0.02795	0.18246
0.936 - 1.014	0.00000	0.00000	0.00000	0.00210	0.03487
1.014 - 1.099	0.00000	0.00000	0.00000	0.00000	0.00225
1.099 - 1.190	0.00000	0.00000	0.00000	0.00000	0.00000

Pulse Height (MeVee)	Neutron Energy				
	2.87 MeV	3.08 MeV	3.32 MeV	3.58 MeV	3.87 MeV
0.057 - 0.067	0.80923	0.73758	0.65519	0.59774	0.53811
0.067 - 0.077	0.75114	0.68245	0.60691	0.56042	0.49885
0.077 - 0.087	0.70402	0.63780	0.57072	0.52341	0.46863
0.087 - 0.097	0.66521	0.60317	0.53721	0.49726	0.44268
0.097 - 0.107	0.64299	0.57047	0.51163	0.47513	0.42246
0.107 - 0.117	0.61970	0.55156	0.48636	0.45529	0.40876
0.117 - 0.127	0.60284	0.53129	0.46805	0.43771	0.39535
0.127 - 0.137	0.58448	0.52027	0.45310	0.42048	0.38224
0.137 - 0.149	0.56709	0.50906	0.44135	0.40808	0.37016
0.149 - 0.161	0.54921	0.49745	0.43409	0.39561	0.35810
0.161 - 0.174	0.53632	0.48361	0.42711	0.38764	0.34814
0.174 - 0.189	0.52485	0.46791	0.41552	0.37785	0.33718
0.189 - 0.205	0.50173	0.44368	0.39082	0.35897	0.31827
0.205 - 0.222	0.48808	0.43347	0.37774	0.34532	0.30859
0.222 - 0.240	0.47750	0.42535	0.37197	0.33750	0.30100
0.240 - 0.260	0.46268	0.41728	0.36551	0.33233	0.29293
0.260 - 0.282	0.44672	0.39943	0.35480	0.32489	0.28596
0.282 - 0.305	0.37996	0.33477	0.29647	0.27453	0.24469
0.305 - 0.331	0.37893	0.33342	0.28982	0.27037	0.24373
0.331 - 0.358	0.43330	0.37905	0.32766	0.30053	0.27417
0.358 - 0.388	0.42685	0.36573	0.31896	0.28945	0.26146
0.388 - 0.421	0.40009	0.32826	0.30055	0.26757	0.23360
0.421 - 0.456	0.39984	0.33385	0.29454	0.26714	0.23142
0.456 - 0.494	0.42545	0.34066	0.30628	0.27398	0.23996
0.494 - 0.535	0.43560	0.34991	0.31182	0.27696	0.23623
0.535 - 0.579	0.49989	0.39761	0.34243	0.30444	0.26469
0.579 - 0.627	0.49910	0.40904	0.35273	0.30862	0.25951
0.627 - 0.680	0.44650	0.38545	0.32749	0.28363	0.24358
0.680 - 0.736	0.39439	0.37639	0.32308	0.28259	0.23524
0.736 - 0.798	0.36663	0.37665	0.34005	0.30291	0.25116
0.798 - 0.864	0.33273	0.33599	0.33389	0.30587	0.25786
0.864 - 0.936	0.30603	0.30871	0.30357	0.30102	0.26714
0.936 - 1.014	0.19845	0.28028	0.26934	0.28126	0.26496
1.014 - 1.099	0.04812	0.20727	0.23864	0.24687	0.24982
1.099 - 1.190	0.00432	0.07676	0.20110	0.21760	0.22297
1.190 - 1.290	0.00000	0.01038	0.10480	0.20052	0.20381
1.290 - 1.397	0.00000	0.00032	0.01895	0.13681	0.18806
1.397 - 1.514	0.00000	0.00000	0.00000	0.03857	0.15787
1.514 - 1.640	0.00000	0.00000	0.00000	0.00322	0.06448
1.640 - 1.741	0.00000	0.00000	0.00000	0.00000	0.01276
1.741 - 1.849	0.00000	0.00000	0.00000	0.00000	0.00186
1.849 - 1.963	0.00000	0.00000	0.00000	0.00000	0.00000

Pulse Height (MeVee)	Neutron Energy				
	4.20 MeV	4.58 MeV	5.01 MeV	5.50 MeV	6.07 MeV
0.057 - 0.067	0.45332	0.40753	0.36565	0.31270	0.29051
0.067 - 0.077	0.41792	0.37534	0.33653	0.28966	0.26862
0.077 - 0.087	0.38651	0.35101	0.31691	0.26959	0.25210
0.087 - 0.097	0.36260	0.32837	0.30011	0.25539	0.23796
0.097 - 0.107	0.34495	0.31063	0.28391	0.24456	0.22472
0.107 - 0.117	0.33218	0.29694	0.27076	0.23214	0.21711
0.117 - 0.127	0.32222	0.28807	0.25905	0.22276	0.20826
0.127 - 0.137	0.31637	0.28039	0.25171	0.21402	0.20015
0.137 - 0.149	0.30769	0.27226	0.24617	0.20599	0.19261
0.149 - 0.161	0.29994	0.26563	0.23957	0.19961	0.18583
0.161 - 0.174	0.29199	0.25730	0.23204	0.19448	0.17948
0.174 - 0.189	0.28239	0.24882	0.22315	0.18628	0.17183
0.189 - 0.205	0.26602	0.23390	0.20825	0.17473	0.16026
0.205 - 0.222	0.25567	0.22504	0.19990	0.16766	0.15264
0.222 - 0.240	0.24791	0.21888	0.19402	0.16291	0.14809
0.240 - 0.260	0.24256	0.21220	0.18838	0.15796	0.14454
0.260 - 0.282	0.23295	0.20432	0.18063	0.15124	0.13907
0.282 - 0.305	0.19805	0.17081	0.15149	0.12612	0.11609
0.305 - 0.331	0.19927	0.16728	0.14824	0.12326	0.11312
0.331 - 0.358	0.22840	0.19020	0.16487	0.13682	0.12602
0.358 - 0.388	0.22161	0.18564	0.15702	0.13047	0.11728
0.388 - 0.421	0.19751	0.16839	0.14053	0.11622	0.10350
0.421 - 0.456	0.19200	0.16629	0.13814	0.11297	0.10044
0.456 - 0.494	0.20084	0.16540	0.14281	0.11367	0.09726
0.494 - 0.535	0.19721	0.16582	0.13942	0.11226	0.09672
0.535 - 0.579	0.21790	0.18263	0.15415	0.12288	0.10399
0.579 - 0.627	0.21987	0.18376	0.15265	0.12450	0.10344
0.627 - 0.680	0.19818	0.16633	0.13695	0.11221	0.09506
0.680 - 0.736	0.19775	0.16232	0.13391	0.10832	0.09168
0.736 - 0.798	0.20718	0.17213	0.13906	0.11146	0.09332
0.798 - 0.864	0.20803	0.17048	0.13887	0.11028	0.09431
0.864 - 0.936	0.21784	0.17451	0.14133	0.11362	0.09306
0.936 - 1.014	0.22131	0.17712	0.14047	0.11217	0.09266
1.014 - 1.099	0.21797	0.17517	0.13836	0.11018	0.09094
1.099 - 1.190	0.21141	0.17625	0.13702	0.10825	0.08677
1.190 - 1.290	0.20882	0.18007	0.14185	0.10971	0.08925
1.290 - 1.397	0.18837	0.18547	0.14862	0.11334	0.09082
1.397 - 1.514	0.17537	0.17967	0.15500	0.11881	0.09556
1.514 - 1.640	0.14217	0.14436	0.13819	0.11122	0.08821
1.640 - 1.741	0.10148	0.13107	0.12830	0.10906	0.08630
1.741 - 1.849	0.05231	0.13476	0.12921	0.12218	0.09926
1.849 - 1.963	0.01199	0.10101	0.12096	0.11669	0.10070
1.963 - 2.085	0.00163	0.04778	0.11545	0.11088	0.10445
2.085 - 2.214	0.00000	0.01037	0.08766	0.10267	0.10056
2.214 - 2.350	0.00000	0.00000	0.04012	0.09630	0.09344
2.350 - 2.496	0.00000	0.00000	0.00868	0.07506	0.08639
2.496 - 2.650	0.00000	0.00000	0.00076	0.03673	0.08216
2.650 - 2.814	0.00000	0.00000	0.00000	0.00894	0.06634
2.814 - 2.988	0.00000	0.00000	0.00000	0.00072	0.03549
2.988 - 3.173	0.00000	0.00000	0.00000	0.00000	0.00966
3.173 - 3.369	0.00000	0.00000	0.00000	0.00000	0.00000

Pulse Height (MeVee)	Neutron Energy				
	6.73 MeV	7.30 MeV	7.73 MeV	8.19 MeV	8.69 MeV
0.057 - 0.067	0.24407	0.25782	0.33759	0.30479	0.28369
0.067 - 0.077	0.22508	0.23849	0.31946	0.29439	0.27845
0.077 - 0.087	0.20993	0.21377	0.29487	0.28086	0.26837
0.087 - 0.097	0.19593	0.19026	0.24495	0.25300	0.25601
0.097 - 0.107	0.18561	0.17137	0.20802	0.20706	0.23267
0.107 - 0.117	0.17786	0.16203	0.18245	0.17395	0.20063
0.117 - 0.127	0.17275	0.15555	0.17218	0.15224	0.17759
0.127 - 0.137	0.16949	0.15158	0.16563	0.14328	0.15977
0.137 - 0.149	0.16373	0.14878	0.16130	0.13782	0.14981
0.149 - 0.161	0.15847	0.14475	0.15713	0.13371	0.14417
0.161 - 0.174	0.15322	0.14051	0.15251	0.12918	0.13872
0.174 - 0.189	0.14781	0.13470	0.14591	0.12388	0.13213
0.189 - 0.205	0.13913	0.12690	0.13655	0.11400	0.12173
0.205 - 0.222	0.13338	0.12253	0.13155	0.10761	0.11193
0.222 - 0.240	0.12915	0.11927	0.12830	0.10392	0.10330
0.240 - 0.260	0.12468	0.11570	0.12486	0.10069	0.09602
0.260 - 0.282	0.11899	0.11059	0.11988	0.09672	0.09030
0.282 - 0.305	0.09928	0.09186	0.09950	0.08096	0.07524
0.305 - 0.331	0.09758	0.08938	0.09702	0.07853	0.07383
0.331 - 0.358	0.10871	0.09952	0.10769	0.08754	0.08168
0.358 - 0.388	0.10240	0.09540	0.10074	0.08262	0.07684
0.388 - 0.421	0.08879	0.08602	0.08654	0.07554	0.06527
0.421 - 0.456	0.08769	0.08653	0.08381	0.07199	0.06536
0.456 - 0.494	0.08814	0.08480	0.08520	0.07627	0.06360
0.494 - 0.535	0.08384	0.08146	0.08333	0.07173	0.06364
0.535 - 0.579	0.09180	0.08739	0.08734	0.07838	0.06626
0.579 - 0.627	0.08775	0.08254	0.08458	0.07750	0.06502
0.627 - 0.680	0.07788	0.07369	0.07206	0.06760	0.06087
0.680 - 0.736	0.07608	0.07120	0.06971	0.06360	0.05661
0.736 - 0.798	0.07805	0.07035	0.06943	0.06240	0.05820
0.798 - 0.864	0.07621	0.06872	0.06734	0.06263	0.05663
0.864 - 0.936	0.07628	0.07014	0.06672	0.05978	0.05617
0.936 - 1.014	0.07526	0.06535	0.06373	0.05751	0.05341
1.014 - 1.099	0.07193	0.06235	0.05913	0.05469	0.05118
1.099 - 1.190	0.06978	0.06117	0.05835	0.05136	0.04818
1.190 - 1.290	0.07118	0.06267	0.05716	0.05151	0.04841
1.290 - 1.397	0.07184	0.06165	0.05835	0.05100	0.04815
1.397 - 1.514	0.07429	0.06239	0.05868	0.05026	0.04866
1.514 - 1.640	0.06755	0.05826	0.05165	0.04472	0.04175
1.640 - 1.741	0.06650	0.05556	0.05034	0.04393	0.04125
1.741 - 1.849	0.07519	0.06219	0.05668	0.04953	0.04434
1.849 - 1.963	0.07574	0.06308	0.05682	0.04825	0.04442
1.963 - 2.085	0.08039	0.06583	0.06055	0.05009	0.04567
2.085 - 2.214	0.08242	0.06689	0.06096	0.04983	0.04596
2.214 - 2.350	0.08230	0.06803	0.06036	0.05109	0.04564
2.350 - 2.496	0.08254	0.07061	0.06155	0.05190	0.04609
2.496 - 2.650	0.07940	0.06957	0.06299	0.05399	0.04641
2.650 - 2.814	0.07471	0.07069	0.06333	0.05546	0.04721
2.814 - 2.988	0.06984	0.06693	0.06469	0.05504	0.04951
2.988 - 3.173	0.06012	0.06289	0.06092	0.05610	0.04921
3.173 - 3.369	0.03731	0.05790	0.05672	0.05435	0.05145
3.369 - 3.578	0.01248	0.05025	0.05126	0.05013	0.04997
3.578 - 3.724	0.00297	0.03010	0.04926	0.04718	0.04769
3.724 - 3.876	0.00054	0.01196	0.04166	0.04724	0.04647
3.876 - 4.034	0.00000	0.00333	0.02354	0.04255	0.04226
4.034 - 4.199	0.00000	0.00000	0.00885	0.03450	0.04020
4.199 - 4.370	0.00000	0.00000	0.00241	0.02142	0.04165
4.370 - 4.548	0.00000	0.00000	0.00000	0.00765	0.03432
4.548 - 4.734	0.00000	0.00000	0.00000	0.00189	0.01649
4.734 - 4.927	0.00000	0.00000	0.00000	0.00000	0.00549
4.927 - 5.128	0.00000	0.00000	0.00000	0.00000	0.00159
5.128 - 5.338	0.00000	0.00000	0.00000	0.00000	0.00000

Pulse Height (MeVee)	Neutron Energy				
	9.24 MeV	9.84 MeV	10.51 MeV	11.25 MeV	12.07 MeV
0.057 - 0.067	0.23820	0.20917	0.27439	0.29155	0.23308
0.067 - 0.077	0.23352	0.20445	0.27253	0.30158	0.25960
0.077 - 0.087	0.22750	0.20049	0.26815	0.30177	0.26835
0.087 - 0.097	0.21986	0.19539	0.26415	0.29763	0.26854
0.097 - 0.107	0.21041	0.18888	0.25987	0.29523	0.26435
0.107 - 0.117	0.19589	0.18161	0.25410	0.29303	0.26323
0.117 - 0.127	0.17832	0.17472	0.24432	0.29008	0.26240
0.127 - 0.137	0.16405	0.16709	0.23353	0.27913	0.26139
0.137 - 0.149	0.15023	0.15788	0.22162	0.26360	0.25441
0.149 - 0.161	0.14110	0.14867	0.20727	0.24537	0.23867
0.161 - 0.174	0.13513	0.13924	0.19384	0.22567	0.22170
0.174 - 0.189	0.12829	0.13182	0.17854	0.20392	0.19798
0.189 - 0.205	0.11790	0.12118	0.16210	0.18077	0.17192
0.205 - 0.222	0.10991	0.11293	0.15084	0.16556	0.15521
0.222 - 0.240	0.10041	0.10579	0.14166	0.15344	0.14241
0.240 - 0.260	0.08907	0.09470	0.13220	0.14323	0.12947
0.260 - 0.282	0.07847	0.07980	0.11753	0.13205	0.11861
0.282 - 0.305	0.06306	0.05861	0.08742	0.10398	0.09505
0.305 - 0.331	0.06128	0.05393	0.07683	0.09372	0.08904
0.331 - 0.358	0.06860	0.05937	0.07953	0.09680	0.09346
0.358 - 0.388	0.06408	0.05627	0.07215	0.08371	0.08423
0.388 - 0.421	0.05763	0.04976	0.06745	0.06870	0.07282
0.421 - 0.456	0.05643	0.05177	0.05678	0.06865	0.06553
0.456 - 0.494	0.05404	0.05232	0.04833	0.06644	0.05703
0.494 - 0.535	0.05405	0.04834	0.04590	0.05055	0.05372
0.535 - 0.579	0.05896	0.05315	0.04962	0.04598	0.05664
0.579 - 0.627	0.05903	0.05344	0.04761	0.04198	0.05582
0.627 - 0.680	0.05304	0.04578	0.04129	0.03834	0.04390
0.680 - 0.736	0.04982	0.04456	0.04067	0.03542	0.03530
0.736 - 0.798	0.05120	0.04575	0.04048	0.03585	0.03297
0.798 - 0.864	0.05008	0.04462	0.04056	0.03627	0.03065
0.864 - 0.936	0.04935	0.04529	0.03901	0.03593	0.03040
0.936 - 1.014	0.04898	0.04291	0.03789	0.03437	0.03048
1.014 - 1.099	0.04728	0.04187	0.03791	0.03310	0.02858
1.099 - 1.190	0.04456	0.03987	0.03573	0.03166	0.02805
1.190 - 1.290	0.04354	0.04054	0.03512	0.03110	0.02739
1.290 - 1.397	0.04229	0.03920	0.03481	0.03112	0.02841
1.397 - 1.514	0.04281	0.03829	0.03641	0.03210	0.02764
1.514 - 1.640	0.03747	0.03518	0.03160	0.02754	0.02398
1.640 - 1.741	0.03602	0.03408	0.03063	0.02680	0.02307
1.741 - 1.849	0.03909	0.03667	0.03273	0.02941	0.02553
1.849 - 1.963	0.03938	0.03646	0.03197	0.02996	0.02515
1.963 - 2.085	0.03999	0.03505	0.03202	0.02846	0.02515
2.085 - 2.214	0.03885	0.03643	0.03276	0.02853	0.02559
2.214 - 2.350	0.03933	0.03575	0.03228	0.02853	0.02522
2.350 - 2.496	0.03848	0.03530	0.03063	0.02902	0.02449
2.496 - 2.650	0.04008	0.03486	0.03130	0.02816	0.02443
2.650 - 2.814	0.04059	0.03454	0.03184	0.02702	0.02445
2.814 - 2.988	0.04088	0.03488	0.03042	0.02689	0.02385
2.988 - 3.173	0.04142	0.03529	0.03087	0.02680	0.02370
3.173 - 3.369	0.04134	0.03570	0.03072	0.02639	0.02350
3.369 - 3.578	0.04199	0.03575	0.03063	0.02659	0.02269
3.578 - 3.724	0.04286	0.03720	0.03125	0.02588	0.02278
3.724 - 3.876	0.04345	0.03686	0.03094	0.02643	0.02245
3.876 - 4.034	0.04067	0.03782	0.03134	0.02570	0.02224
4.034 - 4.199	0.03769	0.03564	0.03092	0.02555	0.02164
4.199 - 4.370	0.03890	0.03839	0.03462	0.02814	0.02420
4.370 - 4.548	0.04027	0.03826	0.03576	0.03126	0.02601
4.548 - 4.734	0.03352	0.03203	0.03151	0.02771	0.02324
4.734 - 4.927	0.02483	0.02970	0.02800	0.02604	0.02143
4.927 - 5.128	0.01513	0.02968	0.02813	0.02640	0.02337
5.128 - 5.338	0.00600	0.02555	0.02841	0.02671	0.02435
5.338 - 5.555	0.00155	0.01475	0.02717	0.02655	0.02447
5.555 - 5.782	0.00000	0.00587	0.02300	0.02498	0.02399
5.782 - 6.018	0.00000	0.00162	0.01424	0.02461	0.02344



6.018 - 6.264	0.00000	0.00000	0.00568	0.02139	0.02180
6.264 - 6.520	0.00000	0.00000	0.00137	0.01374	0.02186
6.520 - 6.786	0.00000	0.00000	0.00000	0.00588	0.02000
6.786 - 7.063	0.00000	0.00000	0.00000	0.00170	0.01362
7.063 - 7.205	0.00000	0.00000	0.00000	0.00008	0.00644
7.205 - 7.351	0.00000	0.00000	0.00000	0.00000	0.00428
7.351 - 7.499	0.00000	0.00000	0.00000	0.00000	0.00293
7.499 - 7.651	0.00000	0.00000	0.00000	0.00000	0.00149
7.651 - 7.805	0.00000	0.00000	0.00000	0.00000	0.00041
7.805 - 7.963	0.00000	0.00000	0.00000	0.00000	0.00000

---

Pulse Height (MeVee)	Neutron Energy				
	12.98 MeV	14.00 MeV	15.14 MeV	16.43 MeV	17.90 MeV
0.057 - 0.067	0.21443	0.20606	0.24406	0.21385	0.18256
0.067 - 0.077	0.23676	0.21941	0.25208	0.21985	0.18418
0.077 - 0.087	0.25114	0.23090	0.25415	0.21887	0.18306
0.087 - 0.097	0.24807	0.23669	0.25512	0.21251	0.17747
0.097 - 0.107	0.24040	0.22355	0.24905	0.20651	0.16766
0.107 - 0.117	0.23216	0.20875	0.23072	0.19697	0.15921
0.117 - 0.127	0.22708	0.19633	0.21423	0.18424	0.15449
0.127 - 0.137	0.22380	0.18619	0.20104	0.17159	0.15036
0.137 - 0.149	0.22134	0.18009	0.19115	0.16071	0.14662
0.149 - 0.161	0.21731	0.17585	0.18481	0.15227	0.14051
0.161 - 0.174	0.20931	0.17255	0.18225	0.14550	0.13411
0.174 - 0.189	0.19855	0.16917	0.17947	0.14209	0.12427
0.189 - 0.205	0.18147	0.16294	0.17308	0.13660	0.11348
0.205 - 0.222	0.17121	0.16302	0.17150	0.13456	0.10869
0.222 - 0.240	0.16404	0.16679	0.17233	0.13346	0.10595
0.240 - 0.260	0.15573	0.17016	0.17484	0.13270	0.10072
0.260 - 0.282	0.14175	0.16640	0.17520	0.13152	0.09362
0.282 - 0.305	0.10921	0.13481	0.15083	0.11363	0.07863
0.305 - 0.331	0.09968	0.11961	0.14905	0.11503	0.07815
0.331 - 0.358	0.10325	0.12103	0.16354	0.13216	0.09030
0.358 - 0.388	0.09079	0.10427	0.14921	0.12851	0.09087
0.388 - 0.421	0.08005	0.08728	0.12712	0.11654	0.07890
0.421 - 0.456	0.07453	0.07624	0.11246	0.11765	0.07964
0.456 - 0.494	0.07280	0.07146	0.10141	0.12348	0.08346
0.494 - 0.535	0.06443	0.06528	0.08418	0.12007	0.08480
0.535 - 0.579	0.06268	0.06325	0.08116	0.12330	0.09433
0.579 - 0.627	0.05635	0.06050	0.06889	0.10334	0.09557
0.627 - 0.680	0.04691	0.04833	0.05734	0.08492	0.08991
0.680 - 0.736	0.04189	0.04076	0.04999	0.06939	0.08465
0.736 - 0.798	0.03955	0.03853	0.04872	0.06192	0.08097
0.798 - 0.864	0.03286	0.03771	0.04399	0.05429	0.06928
0.864 - 0.936	0.02957	0.03857	0.03990	0.04952	0.05953
0.936 - 1.014	0.02750	0.03564	0.03529	0.04104	0.05155
1.014 - 1.099	0.02521	0.02941	0.02998	0.03219	0.04351
1.099 - 1.190	0.02406	0.02384	0.02631	0.02858	0.03800
1.190 - 1.290	0.02348	0.02302	0.02512	0.02829	0.03412
1.290 - 1.397	0.02268	0.02190	0.02112	0.02800	0.03013
1.397 - 1.514	0.02339	0.02270	0.02014	0.02617	0.02707
1.514 - 1.640	0.02090	0.01964	0.01801	0.01897	0.02128
1.640 - 1.741	0.01963	0.01866	0.01667	0.01587	0.01848
1.741 - 1.849	0.02236	0.01975	0.01833	0.01655	0.01935
1.849 - 1.963	0.02130	0.01974	0.01701	0.01619	0.01845
1.963 - 2.085	0.02262	0.01965	0.01727	0.01543	0.01610
2.085 - 2.214	0.02184	0.01995	0.01741	0.01644	0.01548
2.214 - 2.350	0.02122	0.01948	0.01652	0.01523	0.01461
2.350 - 2.496	0.02130	0.01914	0.01656	0.01454	0.01411
2.496 - 2.650	0.02170	0.01943	0.01630	0.01523	0.01327
2.650 - 2.814	0.02095	0.01951	0.01645	0.01489	0.01312
2.814 - 2.988	0.02086	0.01869	0.01637	0.01426	0.01243
2.988 - 3.173	0.02091	0.01843	0.01597	0.01352	0.01276
3.173 - 3.369	0.02032	0.01830	0.01559	0.01348	0.01193
3.369 - 3.578	0.01997	0.01690	0.01514	0.01306	0.01103
3.578 - 3.724	0.01990	0.01754	0.01447	0.01346	0.01078
3.724 - 3.876	0.01922	0.01886	0.01556	0.01313	0.01040
3.876 - 4.034	0.02002	0.01752	0.01389	0.01266	0.01091
4.034 - 4.199	0.01878	0.01639	0.01420	0.01246	0.01026
4.199 - 4.370	0.02053	0.01825	0.01616	0.01362	0.01158
4.370 - 4.548	0.02151	0.01898	0.01588	0.01378	0.01170
4.548 - 4.734	0.01898	0.01672	0.01426	0.01177	0.01018
4.734 - 4.927	0.01783	0.01477	0.01367	0.01138	0.00983
4.927 - 5.128	0.01948	0.01660	0.01397	0.01202	0.01017
5.128 - 5.338	0.01992	0.01717	0.01460	0.01224	0.01019
5.338 - 5.555	0.01963	0.01729	0.01468	0.01254	0.01042
5.555 - 5.782	0.02104	0.01750	0.01466	0.01243	0.01066
5.782 - 6.018	0.02116	0.01828	0.01471	0.01242	0.01029

6.018 - 6.264	0.02130	0.01844	0.01470	0.01243	0.01053
6.264 - 6.520	0.02091	0.01879	0.01559	0.01324	0.01083
6.520 - 6.786	0.02034	0.01940	0.01567	0.01257	0.01083
6.786 - 7.063	0.02010	0.01923	0.01650	0.01327	0.01088
7.063 - 7.205	0.01633	0.01655	0.01413	0.01182	0.00909
7.205 - 7.351	0.01530	0.01653	0.01459	0.01166	0.00945
7.351 - 7.499	0.01396	0.01631	0.01489	0.01152	0.00978
7.499 - 7.651	0.01119	0.01602	0.01460	0.01244	0.00997
7.651 - 7.805	0.00879	0.01638	0.01478	0.01194	0.00986
7.805 - 7.963	0.00593	0.01463	0.01480	0.01260	0.00979
7.963 - 8.124	0.00344	0.01506	0.01473	0.01299	0.01017
8.124 - 8.288	0.00192	0.01234	0.01529	0.01289	0.01022
8.288 - 8.455	0.00086	0.00981	0.01442	0.01324	0.01056
8.455 - 8.626	0.00000	0.00676	0.01402	0.01354	0.01087
8.626 - 8.801	0.00000	0.00455	0.01422	0.01305	0.01082
8.801 - 8.978	0.00000	0.00270	0.01174	0.01326	0.01130
8.978 - 9.160	0.00000	0.00136	0.01071	0.01294	0.01131
9.160 - 9.345	0.00000	0.00027	0.00852	0.01274	0.01158
9.345 - 9.534	0.00000	0.00000	0.00485	0.01006	0.00949
9.534 - 9.725	0.00000	0.00000	0.00295	0.00963	0.00918
9.725 - 9.923	0.00000	0.00000	0.00192	0.00914	0.00926
9.923 - 10.123	0.00000	0.00000	0.00126	0.00821	0.00894
10.123 - 10.328	0.00000	0.00000	0.00041	0.00700	0.00909
10.328 - 10.536	0.00000	0.00000	0.00000	0.00505	0.00981
10.536 - 10.749	0.00000	0.00000	0.00000	0.00369	0.00930
10.749 - 10.966	0.00000	0.00000	0.00000	0.00199	0.00847
10.966 - 11.188	0.00000	0.00000	0.00000	0.00096	0.00781
11.188 - 11.414	0.00000	0.00000	0.00000	0.00027	0.00629
11.414 - 11.644	0.00000	0.00000	0.00000	0.00000	0.00397
11.644 - 11.880	0.00000	0.00000	0.00000	0.00000	0.00281
11.880 - 12.120	0.00000	0.00000	0.00000	0.00000	0.00169
12.120 - 12.364	0.00000	0.00000	0.00000	0.00000	0.00084
12.364 - 12.614	0.00000	0.00000	0.00000	0.00000	0.00048
12.614 - 12.869	0.00000	0.00000	0.00000	0.00000	0.00000

Pulse Height (MeVee)	Neutron Energy				
	19.58 MeV	21.50 MeV	23.14 MeV	24.34 MeV	25.64 MeV
0.057 - 0.067	0.16214	0.19835	0.19752	0.16882	0.17497
0.067 - 0.077	0.15234	0.16843	0.16704	0.14385	0.14858
0.077 - 0.087	0.14786	0.15031	0.14403	0.12349	0.12821
0.087 - 0.097	0.14198	0.13837	0.12969	0.10938	0.11186
0.097 - 0.107	0.13708	0.12732	0.11953	0.10015	0.10125
0.107 - 0.117	0.13175	0.11863	0.10997	0.09282	0.09408
0.117 - 0.127	0.12545	0.11229	0.10249	0.08577	0.08720
0.127 - 0.137	0.12032	0.10911	0.09609	0.08037	0.08120
0.137 - 0.149	0.11582	0.10452	0.09335	0.07593	0.07593
0.149 - 0.161	0.11297	0.10113	0.09018	0.07369	0.07224
0.161 - 0.174	0.10978	0.09858	0.08705	0.07135	0.07013
0.174 - 0.189	0.10553	0.09617	0.08428	0.06825	0.06733
0.189 - 0.205	0.09744	0.09031	0.08024	0.06462	0.06289
0.205 - 0.222	0.09137	0.08585	0.07718	0.06280	0.06095
0.222 - 0.240	0.08748	0.08302	0.07399	0.06075	0.05976
0.240 - 0.260	0.08440	0.08023	0.07167	0.05823	0.05750
0.260 - 0.282	0.08032	0.07609	0.06872	0.05568	0.05463
0.282 - 0.305	0.06610	0.06340	0.05660	0.04653	0.04558
0.305 - 0.331	0.06468	0.06170	0.05531	0.04512	0.04457
0.331 - 0.358	0.07324	0.06921	0.06157	0.05035	0.04933
0.358 - 0.388	0.07272	0.06662	0.05852	0.04774	0.04743
0.388 - 0.421	0.06829	0.05689	0.05224	0.04262	0.04318
0.421 - 0.456	0.06750	0.05647	0.05111	0.04414	0.04158
0.456 - 0.494	0.07086	0.05770	0.04641	0.04002	0.04263
0.494 - 0.535	0.07261	0.05558	0.04812	0.03977	0.04084
0.535 - 0.579	0.08058	0.05984	0.05368	0.04676	0.04584
0.579 - 0.627	0.07989	0.06150	0.05142	0.04313	0.04170
0.627 - 0.680	0.07499	0.05575	0.04624	0.03886	0.03793
0.680 - 0.736	0.07210	0.05469	0.04480	0.03512	0.03628
0.736 - 0.798	0.07685	0.05696	0.04524	0.03620	0.03883
0.798 - 0.864	0.07650	0.05910	0.04276	0.03407	0.03303
0.864 - 0.936	0.07648	0.06330	0.04519	0.03505	0.03376
0.936 - 1.014	0.06790	0.06681	0.04552	0.03100	0.03158
1.014 - 1.099	0.05627	0.06664	0.04350	0.03161	0.03055
1.099 - 1.190	0.04789	0.06423	0.04501	0.03247	0.03002
1.190 - 1.290	0.04315	0.06198	0.04900	0.03486	0.02833
1.290 - 1.397	0.03933	0.05611	0.05345	0.03686	0.02951
1.397 - 1.514	0.03734	0.04831	0.05265	0.04050	0.03505
1.514 - 1.640	0.03031	0.03738	0.04597	0.03764	0.03040
1.640 - 1.741	0.02662	0.03084	0.03854	0.03444	0.02917
1.741 - 1.849	0.02764	0.03133	0.03528	0.03731	0.03395
1.849 - 1.963	0.02517	0.02807	0.03513	0.03297	0.03513
1.963 - 2.085	0.02477	0.02510	0.02634	0.03004	0.03234
2.085 - 2.214	0.02375	0.02388	0.02620	0.02633	0.03193
2.214 - 2.350	0.01981	0.02311	0.02250	0.02359	0.02560
2.350 - 2.496	0.01671	0.02128	0.02063	0.01985	0.02435
2.496 - 2.650	0.01507	0.02092	0.02056	0.01742	0.02088
2.650 - 2.814	0.01397	0.01831	0.01881	0.01602	0.01782
2.814 - 2.988	0.01404	0.01697	0.01859	0.01633	0.01518
2.988 - 3.173	0.01318	0.01390	0.01733	0.01454	0.01362
3.173 - 3.369	0.01211	0.01291	0.01574	0.01350	0.01317
3.369 - 3.578	0.01096	0.01216	0.01388	0.01243	0.01355
3.578 - 3.724	0.01042	0.01099	0.01378	0.01173	0.01298
3.724 - 3.876	0.01071	0.01100	0.01251	0.01018	0.01128
3.876 - 4.034	0.01010	0.00980	0.01147	0.00970	0.01062
4.034 - 4.199	0.00934	0.00986	0.01066	0.00970	0.00982
4.199 - 4.370	0.01086	0.01039	0.01106	0.01087	0.01013
4.370 - 4.548	0.01067	0.01114	0.01085	0.01174	0.01062
4.548 - 4.734	0.00973	0.00820	0.00912	0.00889	0.00838
4.734 - 4.927	0.00836	0.00813	0.00802	0.00702	0.00841
4.927 - 5.128	0.00916	0.00842	0.00828	0.00751	0.00971
5.128 - 5.338	0.00957	0.00848	0.00844	0.00783	0.00937
5.338 - 5.555	0.00956	0.00814	0.00830	0.00717	0.00821
5.555 - 5.782	0.00941	0.00835	0.00812	0.00691	0.00768
5.782 - 6.018	0.00946	0.00776	0.00805	0.00675	0.00752

6.018 - 6.264	0.00961	0.00848	0.00753	0.00703	0.00690
6.264 - 6.520	0.00980	0.00827	0.00690	0.00665	0.00659
6.520 - 6.786	0.00975	0.00810	0.00709	0.00644	0.00730
6.786 - 7.063	0.00981	0.00839	0.00746	0.00616	0.00677
7.063 - 7.205	0.00850	0.00726	0.00651	0.00453	0.00619
7.205 - 7.351	0.00831	0.00720	0.00610	0.00551	0.00653
7.351 - 7.499	0.00881	0.00712	0.00676	0.00487	0.00495
7.499 - 7.651	0.00864	0.00768	0.00744	0.00566	0.00494
7.651 - 7.805	0.00862	0.00738	0.00656	0.00509	0.00515
7.805 - 7.963	0.00871	0.00816	0.00651	0.00535	0.00496
7.963 - 8.124	0.00914	0.00786	0.00606	0.00578	0.00536
8.124 - 8.288	0.00909	0.00753	0.00655	0.00489	0.00503
8.288 - 8.455	0.00949	0.00793	0.00690	0.00528	0.00489
8.455 - 8.626	0.00936	0.00725	0.00644	0.00551	0.00459
8.626 - 8.801	0.00930	0.00771	0.00667	0.00538	0.00508
8.801 - 8.978	0.00973	0.00822	0.00710	0.00556	0.00466
8.978 - 9.160	0.00938	0.00798	0.00711	0.00567	0.00481
9.160 - 9.345	0.00943	0.00789	0.00693	0.00504	0.00528
9.345 - 9.534	0.00805	0.00685	0.00574	0.00434	0.00415
9.534 - 9.726	0.00803	0.00654	0.00564	0.00432	0.00412
9.726 - 9.923	0.00803	0.00649	0.00545	0.00454	0.00470
9.923 - 10.123	0.00798	0.00678	0.00537	0.00429	0.00400
10.123 - 10.328	0.00853	0.00640	0.00609	0.00448	0.00409
10.328 - 10.536	0.00934	0.00698	0.00560	0.00433	0.00438
10.536 - 10.749	0.00891	0.00744	0.00614	0.00499	0.00427
10.749 - 10.966	0.00924	0.00759	0.00594	0.00479	0.00417
10.966 - 11.188	0.00921	0.00721	0.00583	0.00473	0.00428
11.188 - 11.414	0.00935	0.00746	0.00613	0.00478	0.00485
11.414 - 11.644	0.00832	0.00670	0.00532	0.00441	0.00385
11.644 - 11.880	0.00734	0.00652	0.00512	0.00378	0.00383
11.880 - 12.120	0.00710	0.00663	0.00517	0.00417	0.00413
12.120 - 12.364	0.00626	0.00606	0.00537	0.00398	0.00387
12.364 - 12.614	0.00540	0.00632	0.00522	0.00405	0.00368
12.614 - 12.869	0.00425	0.00619	0.00519	0.00406	0.00359
12.869 - 13.129	0.00280	0.00565	0.00464	0.00364	0.00324
13.129 - 13.394	0.00206	0.00572	0.00471	0.00352	0.00337
13.394 - 13.665	0.00126	0.00513	0.00446	0.00374	0.00311
13.665 - 13.941	0.00079	0.00459	0.00451	0.00387	0.00330
13.941 - 14.223	0.00032	0.00400	0.00396	0.00379	0.00346
14.223 - 14.510	0.00000	0.00313	0.00483	0.00395	0.00346
14.510 - 14.803	0.00000	0.00261	0.00440	0.00361	0.00302
14.803 - 15.102	0.00000	0.00158	0.00461	0.00387	0.00343
15.102 - 15.407	0.00000	0.00099	0.00405	0.00385	0.00326
15.407 - 15.718	0.00000	0.00000	0.00295	0.00386	0.00366
15.718 - 16.036	0.00000	0.00000	0.00178	0.00275	0.00261
16.036 - 16.360	0.00000	0.00000	0.00106	0.00257	0.00279
16.360 - 16.690	0.00000	0.00000	0.00054	0.00193	0.00260
16.690 - 17.028	0.00000	0.00000	0.00000	0.00161	0.00298
17.028 - 17.372	0.00000	0.00000	0.00000	0.00107	0.00247
17.372 - 17.723	0.00000	0.00000	0.00000	0.00000	0.00216
17.723 - 18.081	0.00000	0.00000	0.00000	0.00000	0.00126
18.081 - 18.446	0.00000	0.00000	0.00000	0.00000	0.00087
18.446 - 18.819	0.00000	0.00000	0.00000	0.00000	0.00000

Pulse Height (MeVee)	Neutron Energy				
	27.04 MeV	28.57 MeV	30.23 MeV	32.04 MeV	34.02 MeV
0.057 - 0.067	0.17576	0.20091	0.18276	0.23468	0.19325
0.067 - 0.077	0.14830	0.16786	0.15308	0.19512	0.16213
0.077 - 0.087	0.12922	0.14593	0.13090	0.16687	0.13754
0.087 - 0.097	0.11216	0.12780	0.11622	0.14626	0.11987
0.097 - 0.107	0.09973	0.11288	0.10247	0.13063	0.10719
0.107 - 0.117	0.09164	0.10206	0.09154	0.11667	0.09605
0.117 - 0.127	0.08557	0.09446	0.08341	0.10537	0.08644
0.127 - 0.137	0.07952	0.08885	0.07787	0.09642	0.07845
0.137 - 0.149	0.07416	0.08194	0.07290	0.09020	0.07225
0.149 - 0.161	0.06959	0.07673	0.06771	0.08443	0.06740
0.161 - 0.174	0.06634	0.07206	0.06365	0.07872	0.06313
0.174 - 0.189	0.06403	0.06855	0.05900	0.07282	0.05842
0.189 - 0.205	0.05962	0.06440	0.05492	0.06614	0.05251
0.205 - 0.222	0.05725	0.06124	0.05257	0.06323	0.04897
0.222 - 0.240	0.05604	0.05956	0.05060	0.06102	0.04726
0.240 - 0.260	0.05496	0.05817	0.04912	0.05876	0.04567
0.260 - 0.282	0.05190	0.05620	0.04758	0.05643	0.04323
0.282 - 0.305	0.04323	0.04623	0.03994	0.04769	0.03633
0.305 - 0.331	0.04227	0.04523	0.03846	0.04661	0.03613
0.331 - 0.358	0.04698	0.05049	0.04290	0.05143	0.04031
0.358 - 0.388	0.04491	0.04742	0.04257	0.04782	0.03921
0.388 - 0.421	0.04097	0.04199	0.04298	0.03879	0.03942
0.421 - 0.456	0.04157	0.03829	0.04060	0.03874	0.03363
0.456 - 0.494	0.03924	0.03856	0.04087	0.03723	0.03706
0.494 - 0.535	0.03510	0.03522	0.03826	0.03636	0.03495
0.535 - 0.579	0.04186	0.03914	0.04183	0.03547	0.03687
0.579 - 0.627	0.03919	0.03791	0.03909	0.03895	0.03599
0.627 - 0.680	0.03477	0.03428	0.03328	0.03271	0.03201
0.680 - 0.736	0.03233	0.02928	0.03056	0.03014	0.02836
0.736 - 0.798	0.03113	0.03313	0.03160	0.03025	0.03029
0.798 - 0.864	0.03178	0.02986	0.03044	0.02947	0.03011
0.864 - 0.936	0.03068	0.02995	0.02888	0.02888	0.02820
0.936 - 1.014	0.02930	0.02789	0.02844	0.02598	0.02563
1.014 - 1.099	0.02796	0.02502	0.02481	0.02503	0.02434
1.099 - 1.190	0.02578	0.02395	0.02397	0.02357	0.02362
1.190 - 1.290	0.02474	0.02352	0.02292	0.02316	0.02300
1.290 - 1.397	0.02603	0.02279	0.02199	0.02197	0.02451
1.397 - 1.514	0.02633	0.02239	0.02268	0.02181	0.02203
1.514 - 1.640	0.02466	0.02010	0.01915	0.01806	0.01970
1.640 - 1.741	0.02411	0.01889	0.01773	0.01692	0.01898
1.741 - 1.849	0.02782	0.02183	0.01956	0.01886	0.01947
1.849 - 1.963	0.02753	0.02137	0.01766	0.01657	0.01884
1.963 - 2.085	0.02942	0.02284	0.01922	0.01683	0.01868
2.085 - 2.214	0.02814	0.02330	0.02004	0.01809	0.01648
2.214 - 2.350	0.02842	0.02313	0.01976	0.01693	0.01667
2.350 - 2.496	0.02454	0.02247	0.02004	0.01591	0.01623
2.496 - 2.650	0.02315	0.02286	0.01971	0.01717	0.01494
2.650 - 2.814	0.01980	0.02052	0.01974	0.01621	0.01451
2.814 - 2.988	0.01741	0.01847	0.01855	0.01652	0.01561
2.988 - 3.173	0.01553	0.01639	0.01778	0.01560	0.01456
3.173 - 3.369	0.01345	0.01500	0.01626	0.01562	0.01455
3.369 - 3.578	0.01181	0.01329	0.01377	0.01364	0.01431
3.578 - 3.724	0.01137	0.01141	0.01226	0.01242	0.01336
3.724 - 3.876	0.01163	0.01073	0.01162	0.01203	0.01339
3.876 - 4.034	0.01107	0.01048	0.00983	0.01107	0.01138
4.034 - 4.199	0.01008	0.00991	0.00935	0.00978	0.01030
4.199 - 4.370	0.01085	0.01047	0.01002	0.01017	0.01082
4.370 - 4.548	0.01083	0.01009	0.01091	0.00957	0.01185
4.548 - 4.734	0.00884	0.00808	0.00879	0.00858	0.00862
4.734 - 4.927	0.00785	0.00774	0.00776	0.00737	0.00806
4.927 - 5.128	0.00819	0.00768	0.00820	0.00733	0.00793
5.128 - 5.338	0.00841	0.00750	0.00842	0.00732	0.00801
5.338 - 5.555	0.00781	0.00738	0.00762	0.00717	0.00744
5.555 - 5.782	0.00808	0.00789	0.00695	0.00755	0.00792
5.782 - 6.018	0.00825	0.00716	0.00659	0.00727	0.00676

6.018 - 6.264	0.00796	0.00712	0.00772	0.00733	0.00672
6.264 - 6.520	0.00726	0.00722	0.00730	0.00610	0.00691
6.520 - 6.786	0.00675	0.00740	0.00684	0.00662	0.00693
6.786 - 7.063	0.00606	0.00766	0.00715	0.00597	0.00688
7.063 - 7.205	0.00580	0.00691	0.00641	0.00565	0.00577
7.205 - 7.351	0.00506	0.00617	0.00622	0.00589	0.00553
7.351 - 7.499	0.00515	0.00637	0.00637	0.00561	0.00588
7.499 - 7.651	0.00537	0.00604	0.00616	0.00584	0.00573
7.651 - 7.805	0.00511	0.00569	0.00615	0.00614	0.00527
7.805 - 7.963	0.00543	0.00597	0.00624	0.00588	0.00569
7.963 - 8.124	0.00578	0.00493	0.00606	0.00599	0.00591
8.124 - 8.288	0.00557	0.00499	0.00699	0.00611	0.00630
8.288 - 8.455	0.00519	0.00512	0.00586	0.00566	0.00692
8.455 - 8.626	0.00506	0.00499	0.00566	0.00556	0.00486
8.626 - 8.801	0.00473	0.00551	0.00555	0.00622	0.00599
8.801 - 8.978	0.00488	0.00525	0.00496	0.00655	0.00586
8.978 - 9.160	0.00414	0.00532	0.00451	0.00595	0.00589
9.160 - 9.345	0.00473	0.00471	0.00486	0.00609	0.00595
9.345 - 9.534	0.00374	0.00352	0.00405	0.00492	0.00473
9.534 - 9.726	0.00358	0.00356	0.00334	0.00435	0.00454
9.726 - 9.923	0.00372	0.00361	0.00365	0.00473	0.00501
9.923 - 10.123	0.00378	0.00379	0.00396	0.00418	0.00493
10.123 - 10.328	0.00350	0.00298	0.00323	0.00410	0.00520
10.328 - 10.536	0.00372	0.00313	0.00386	0.00399	0.00522
10.536 - 10.749	0.00387	0.00372	0.00359	0.00373	0.00480
10.749 - 10.966	0.00383	0.00320	0.00375	0.00318	0.00514
10.966 - 11.188	0.00353	0.00300	0.00363	0.00359	0.00453
11.188 - 11.414	0.00382	0.00333	0.00337	0.00370	0.00469
11.414 - 11.644	0.00334	0.00351	0.00291	0.00284	0.00396
11.644 - 11.880	0.00328	0.00295	0.00276	0.00292	0.00336
11.880 - 12.120	0.00320	0.00268	0.00241	0.00297	0.00316
12.120 - 12.364	0.00311	0.00269	0.00288	0.00253	0.00296
12.364 - 12.614	0.00354	0.00254	0.00244	0.00273	0.00262
12.614 - 12.869	0.00335	0.00279	0.00240	0.00269	0.00286
12.869 - 13.129	0.00292	0.00237	0.00254	0.00227	0.00258
13.129 - 13.394	0.00274	0.00262	0.00240	0.00203	0.00239
13.394 - 13.665	0.00288	0.00243	0.00227	0.00209	0.00226
13.665 - 13.941	0.00274	0.00245	0.00228	0.00204	0.00219
13.941 - 14.223	0.00251	0.00247	0.00234	0.00214	0.00191
14.223 - 14.510	0.00273	0.00230	0.00194	0.00222	0.00218
14.510 - 14.803	0.00312	0.00202	0.00214	0.00219	0.00219
14.803 - 15.102	0.00283	0.00236	0.00202	0.00226	0.00195
15.102 - 15.407	0.00310	0.00229	0.00251	0.00179	0.00197
15.407 - 15.718	0.00306	0.00260	0.00201	0.00191	0.00191
15.718 - 16.036	0.00242	0.00207	0.00205	0.00156	0.00147
16.036 - 16.360	0.00236	0.00168	0.00168	0.00147	0.00156
16.360 - 16.690	0.00246	0.00205	0.00158	0.00165	0.00146
16.690 - 17.028	0.00250	0.00216	0.00190	0.00169	0.00148
17.028 - 17.372	0.00253	0.00208	0.00177	0.00163	0.00146
17.372 - 17.723	0.00238	0.00230	0.00176	0.00159	0.00137
17.723 - 18.081	0.00216	0.00182	0.00154	0.00129	0.00126
18.081 - 18.446	0.00164	0.00156	0.00129	0.00127	0.00120
18.446 - 18.819	0.00181	0.00169	0.00119	0.00123	0.00119
18.819 - 19.199	0.00111	0.00143	0.00119	0.00123	0.00101
19.199 - 19.587	0.00062	0.00116	0.00102	0.00079	0.00067
19.587 - 19.982	0.00018	0.00095	0.00112	0.00083	0.00072
19.982 - 20.386	0.00000	0.00104	0.00101	0.00089	0.00096
20.386 - 20.798	0.00000	0.00123	0.00171	0.00169	0.00137
20.798 - 21.218	0.00000	0.00000	0.00160	0.00152	0.00108
21.218 - 21.647	0.00000	0.00000	0.00130	0.00163	0.00130
21.647 - 22.084	0.00000	0.00000	0.00079	0.00101	0.00102
22.084 - 22.530	0.00000	0.00000	0.00045	0.00102	0.00089
22.530 - 22.985	0.00000	0.00000	0.00000	0.00083	0.00099
22.985 - 23.450	0.00000	0.00000	0.00000	0.00064	0.00077
23.450 - 23.923	0.00000	0.00000	0.00000	0.00040	0.00073
23.923 - 24.407	0.00000	0.00000	0.00000	0.00000	0.00056
24.407 - 24.900	0.00000	0.00000	0.00000	0.00000	0.00045
24.900 - 25.403	0.00000	0.00000	0.00000	0.00000	0.00050
25.403 - 25.916	0.00000	0.00000	0.00000	0.00000	0.00036
25.916 - 26.439	0.00000	0.00000	0.00000	0.00000	0.00000

Pulse Height (MeVee)	Neutron Energy		
	36.20 MeV	38.60 MeV	41.25 MeV
0.057 - 0.067	0.24837	0.28180	0.32426
0.067 - 0.077	0.20845	0.23242	0.26330
0.077 - 0.087	0.17785	0.20022	0.22439
0.087 - 0.097	0.15434	0.17177	0.19585
0.097 - 0.107	0.13571	0.15191	0.17186
0.107 - 0.117	0.12330	0.13527	0.15240
0.117 - 0.127	0.11132	0.12399	0.13749
0.127 - 0.137	0.10022	0.11217	0.12590
0.137 - 0.149	0.09108	0.10110	0.11437
0.149 - 0.161	0.08402	0.09237	0.10358
0.161 - 0.174	0.07883	0.08511	0.09478
0.174 - 0.189	0.07288	0.07897	0.08656
0.189 - 0.205	0.06555	0.07129	0.07799
0.205 - 0.222	0.06047	0.06536	0.07181
0.222 - 0.240	0.05673	0.06092	0.06669
0.240 - 0.260	0.05508	0.05717	0.06246
0.260 - 0.282	0.05237	0.05502	0.05824
0.282 - 0.305	0.04338	0.04546	0.04859
0.305 - 0.331	0.04280	0.04389	0.04708
0.331 - 0.358	0.04820	0.04971	0.05228
0.358 - 0.388	0.04575	0.04908	0.05078
0.388 - 0.421	0.03926	0.04423	0.04638
0.421 - 0.456	0.03839	0.03720	0.04290
0.456 - 0.494	0.03739	0.03714	0.04058
0.494 - 0.535	0.03431	0.03781	0.03719
0.535 - 0.579	0.03640	0.03994	0.04320
0.579 - 0.627	0.03884	0.03527	0.04375
0.627 - 0.680	0.03176	0.02765	0.03363
0.680 - 0.736	0.02927	0.03186	0.03136
0.736 - 0.798	0.02667	0.02659	0.03029
0.798 - 0.864	0.02608	0.02864	0.02865
0.864 - 0.936	0.02806	0.02552	0.02804
0.936 - 1.014	0.02754	0.02543	0.02696
1.014 - 1.099	0.02723	0.02343	0.02473
1.099 - 1.190	0.02272	0.02492	0.02216
1.190 - 1.290	0.02188	0.02172	0.02274
1.290 - 1.397	0.02111	0.02031	0.02181
1.397 - 1.514	0.02273	0.02257	0.02078
1.514 - 1.640	0.01885	0.01676	0.01743
1.640 - 1.741	0.01664	0.01637	0.01839
1.741 - 1.849	0.01821	0.01990	0.01806
1.849 - 1.963	0.01953	0.01720	0.01876
1.963 - 2.085	0.01747	0.01830	0.01657
2.085 - 2.214	0.01852	0.01760	0.01838
2.214 - 2.350	0.01653	0.01683	0.01632
2.350 - 2.496	0.01473	0.01765	0.01637
2.496 - 2.650	0.01562	0.01597	0.01563
2.650 - 2.814	0.01477	0.01475	0.01498
2.814 - 2.988	0.01409	0.01499	0.01418
2.988 - 3.173	0.01332	0.01341	0.01420
3.173 - 3.369	0.01371	0.01317	0.01324
3.369 - 3.578	0.01306	0.01280	0.01121
3.578 - 3.724	0.01228	0.01065	0.01159
3.724 - 3.876	0.01364	0.01055	0.01046
3.876 - 4.034	0.01188	0.01024	0.01073
4.034 - 4.199	0.01225	0.01041	0.00909
4.199 - 4.370	0.01286	0.01083	0.01087
4.370 - 4.548	0.01156	0.01301	0.01111
4.548 - 4.734	0.01006	0.01156	0.00987
4.734 - 4.927	0.00761	0.00915	0.00980
4.927 - 5.128	0.00773	0.00957	0.00954
5.128 - 5.338	0.00808	0.00873	0.00844
5.338 - 5.555	0.00795	0.00853	0.00905
5.555 - 5.782	0.00752	0.00836	0.00824
5.782 - 6.018	0.00695	0.00800	0.00892



6.018 - 6.264	0.00664	0.00705	0.00819
6.264 - 6.520	0.00649	0.00711	0.00844
6.520 - 6.786	0.00727	0.00707	0.00776
6.786 - 7.063	0.00623	0.00674	0.00687
7.063 - 7.205	0.00497	0.00582	0.00646
7.205 - 7.351	0.00606	0.00589	0.00613
7.351 - 7.499	0.00526	0.00524	0.00546
7.499 - 7.651	0.00551	0.00615	0.00504
7.651 - 7.805	0.00567	0.00572	0.00513
7.805 - 7.963	0.00529	0.00665	0.00564
7.963 - 8.124	0.00550	0.00581	0.00700
8.124 - 8.288	0.00553	0.00551	0.00573
8.288 - 8.455	0.00558	0.00583	0.00610
8.455 - 8.626	0.00564	0.00520	0.00488
8.626 - 8.801	0.00503	0.00622	0.00538
8.801 - 8.978	0.00546	0.00547	0.00553
8.978 - 9.160	0.00566	0.00544	0.00549
9.160 - 9.345	0.00540	0.00486	0.00452
9.345 - 9.534	0.00500	0.00478	0.00412
9.534 - 9.726	0.00411	0.00415	0.00391
9.726 - 9.923	0.00443	0.00439	0.00416
9.923 - 10.123	0.00496	0.00463	0.00392
10.123 - 10.328	0.00472	0.00413	0.00410
10.328 - 10.536	0.00465	0.00448	0.00511
10.536 - 10.749	0.00535	0.00508	0.00486
10.749 - 10.966	0.00426	0.00443	0.00443
10.966 - 11.188	0.00492	0.00396	0.00442
11.188 - 11.414	0.00441	0.00444	0.00404
11.414 - 11.644	0.00405	0.00358	0.00388
11.644 - 11.880	0.00388	0.00384	0.00395
11.880 - 12.120	0.00439	0.00368	0.00379
12.120 - 12.364	0.00434	0.00455	0.00316
12.364 - 12.614	0.00382	0.00379	0.00398
12.614 - 12.869	0.00361	0.00384	0.00317
12.869 - 13.129	0.00327	0.00348	0.00341
13.129 - 13.394	0.00292	0.00324	0.00325
13.394 - 13.665	0.00248	0.00325	0.00321
13.665 - 13.941	0.00239	0.00328	0.00336
13.941 - 14.223	0.00234	0.00345	0.00260
14.223 - 14.510	0.00227	0.00357	0.00301
14.510 - 14.803	0.00231	0.00363	0.00270
14.803 - 15.102	0.00255	0.00288	0.00345
15.102 - 15.407	0.00222	0.00309	0.00305
15.407 - 15.718	0.00209	0.00253	0.00325
15.718 - 16.036	0.00152	0.00188	0.00260
16.036 - 16.360	0.00131	0.00182	0.00268
16.360 - 16.690	0.00141	0.00121	0.00246
16.690 - 17.028	0.00152	0.00153	0.00240
17.028 - 17.372	0.00133	0.00139	0.00238
17.372 - 17.723	0.00169	0.00160	0.00184
17.723 - 18.081	0.00106	0.00133	0.00159
18.081 - 18.446	0.00106	0.00119	0.00113
18.446 - 18.819	0.00086	0.00102	0.00123
18.819 - 19.199	0.00082	0.00077	0.00099
19.199 - 19.587	0.00055	0.00058	0.00089
19.587 - 19.982	0.00062	0.00062	0.00059
19.982 - 20.386	0.00078	0.00079	0.00069
20.386 - 20.798	0.00110	0.00111	0.00137
20.798 - 21.218	0.00113	0.00122	0.00144
21.218 - 21.647	0.00100	0.00092	0.00099
21.647 - 22.084	0.00084	0.00094	0.00065
22.084 - 22.530	0.00078	0.00072	0.00051
22.530 - 22.985	0.00078	0.00079	0.00065
22.985 - 23.450	0.00064	0.00065	0.00071
23.450 - 23.923	0.00069	0.00053	0.00058
23.923 - 24.407	0.00047	0.00063	0.00042
24.407 - 24.900	0.00056	0.00037	0.00036
24.900 - 25.403	0.00043	0.00038	0.00045

25.403 - 25.916	0.00054	0.00049	0.00035
25.916 - 26.439	0.00047	0.00033	0.00033
26.439 - 26.974	0.00039	0.00052	0.00037
26.974 - 27.513	0.00043	0.00038	0.00039
27.513 - 28.074	0.00000	0.00041	0.00035
28.074 - 28.642	0.00000	0.00036	0.00027
28.642 - 29.220	0.00000	0.00000	0.00034
29.220 - 29.810	0.00000	0.00000	0.00017
29.810 - 30.413	0.00000	0.00000	0.00021
30.413 - 31.027	0.00000	0.00000	0.00017
31.027 - 31.654	0.00000	0.00000	0.00018
31.654 - 32.293	0.00000	0.00000	0.00007
32.293 - 32.946	0.00000	0.00000	0.00000

---